Continuum mechanics at nanoscale. A tool to study trees' watering and recovery

Henri Gouin

Accepted in "Rendiconti Lincei - Matematica et Applicazioni (2017)"
Chapter 41 - Mathematical Biology

Continuum mechanics at nanoscale : A tool to study trees' watering and recovery

Henri Gouin

Aix-Marseille Univ, Centrale Marseille, CNRS, M2P2 UMR 7340, 13451 Marseille France

E-mail: henri.gouin@univ-amu.fr, henri.gouin@yahoo.fr

In memory of Professor Giuseppe Grioli

Abstract

The cohesion-tension theory expounds the crude sap ascent thanks to the negative pressure generated by evaporation of water from leaves. Nevertheless, trees pose multiple challenges and seem to live in unphysical conditions: the negative pressure increases cavitation; it is possible to obtain a water equilibrium between connected parts where one is at a positive pressure and the other one is at negative pressure; no theory is able to satisfactorily account for the refilling of vessels after embolism events.

A theoretical form of our paper [49] in the Journal of Theoretical Biology is proposed together with new results: a continuum mechanics model of the disjoining pressure concept refers to the Derjaguin school of physical chemistry. A comparison between liquid behaviour both in tight-filled microtubes and in liquid thin-films is offered when the pressure is negative in liquid bulks and is positive in liquid thin-films and vapour bulks. In embolized xylem microtubes, when the air-vapour pocket pressure is greater than the air-vapour bulk pressure, a refilling flow occurs between the air-vapour domains to empty the air-vapour pockets although the liquid-bulk pressure remains negative. The model has a limit of validity taking the maximal size of trees into account.
These results drop an inkling that the disjoining pressure is an efficient tool to study biological liquids in contact with substrates at a nanoscale range.

PACS numbers: 68.65.k; 82.45.Mp; 87.10.+e; 87.15.Kg; 87.15.La

1 Introduction

Trees are engines running on water, but unlike animals, plants miss an active pump to move liquids along their vascular system. The crude sap contains diluted salts and ascents from roots to leaves thanks to the water evaporation from leaves; its physical properties are roughly those of water. The flow is driven along of xylem microtubes made of dead cells which constitute a watering network. Hydrodynamics, capillarity and osmotic pressure induce the crude sap ascent of a few tens of meters only [106]; nevertheless a sequoia of 115.55 meters height is living in California [79]. Additively, trees

operate a second vascular system - phloem sieve tubes - for the circulation of metabolites through their living tissues and elaborated sap flows passing from leaves to roots.
Measurements of the pressure within the terminal xylem vessels illustrate an extraordinary consequence of the tree behaviour for moving water: the liquid water is under tension. An experimental checking comes from an apparatus called Scholander pressure chamber (see Fig.1, [84]). The pressure difference across plants can easily be of the order

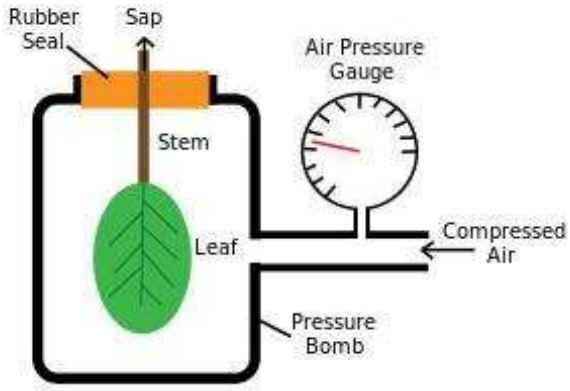

Figure 1: Sketch of the Scholander pressure chamber. A leaf attached to a stem is placed inside a sealed chamber. Compressed air is slowly added to the chamber. As the pressure increases to a convenient level, the sap is forced out of the xylem and is visible at the cut end of the stem. The required pressure is opposite and of equal magnitude to the water pressure in the water-storing tracheids in the leaf.

of 1 to 10 MPa [69]. Although trees do not approach the ultimate tensile strength of liquid water during transpiration [51], multiple types of measurements provide evidence for cavitation of liquid water in the xylem microtubes and cavitation events have been acoustically detected with ultrasonic transducers pressed against the external surface of trees [70, 98]. The porous vessel walls can prevent the bubbles from spreading [68] and the principal flow of water during transpiration goes to evaporation through stomata on the underside of leaves. The pores - or bordered pits - connecting adjacent segments in the xylem vessels pass through the vessel walls, and are bifurcated by bordered-pit membranes which are thin physical fluid-transmitters. No vessels are continuous from roots to petioles, and the water does not leave the vessels in the axial direction but laterally along a long stretch [74]. When wetted on both sides, the bordered-pit membranes allow the liquid-water flow to pass through. In the leaves, the membranes serve as capillary seals; in the stems, the bordered-pit membranes also serve as seals between a gas-filled segment and an adjacent liquid-filled segment avoiding propagation of massive embolisms [95]. Consequently, trees seem to live in unphysical conditions [111]; to be hydrated, they exploit liquid water in metastable states at negative pressure [54].

A classical explanation of the sap ascent phenomenon in tall trees is the *cohesion-tension theory* propounded in 1893-1895 by Boehm, Dixon and Joly and Askenasy [1, 7, 25], followed by an analysis of the sap motion propounded by van der Honert [99]. According to this theory, the crude sap tightly fills microtubes of dead xylem cells and its transport is due to a gradient of negative pressure producing the traction nec-

essary to lift water against gravity. The decrease in negative pressure is related to the closing of aperture of microscopic stomata in leaves through which water vapour is lost by transpiration. The considered aperture is about 2 μm - or less at the top of tall trees as suggested in [59, 80] - which is the right size to prevent cavitation for nucleus germs of the same order of magnitude. Nonetheless, several objections question the validity of the cohesion-tension theory, and worse, preclude the possibility of refilling embolized xylem tubes. To this goal, we first refer to the textbook by Zimmermann [106]. He said:
The heartwood is referred to as a wet wood. It may contain liquid under positive pressure while in the sapwood the transpiration stream moves along a gradient of negative pressures. Why is the water of the central wet core not drawn into the sapwood? The heartwood is relatively dry i.e. most tracheids are embolized. It is rather ironic that a wound in the wet wood area, which bleeds liquid for a long period of time, thus appears to have the transpiration stream as a source of water, in spite of the fact that the pressure of the transpiration stream is negative most of the time. It should be quite clear by now that a drop in xylem pressure below a critical level causes cavitations and normally puts the xylem out of function permanently.
At great elevation, the value of the negative pressure increases risks of cavitation and consequently, the formation of embolisms may cause a definitive break-down of continuous columns of sap inducing leaf death. Crude sap is a fluid with superficial tension lower than superficial tension γ of the pure water, which is about 72.5×10^3 N.m^{-1} at 20° Celsius [69]; if we consider a microscopic air-vapour bubble with a diameter $2R$ smaller than xylem microtube diameters, the difference between air-vapour pressure $\wp_v$ and liquid sap pressure $\wp_l$ is expressed by Young-Laplace formula $\wp_v - \wp_l = 2\gamma/R$; the air-vapour pressure is positive and consequently unstable bubbles will appear when $R \geq -2\gamma/\wp_l$. For a negative pressure $\wp_l = -0.6$ MPa in the sap, corresponding to an approximative minimal value of the hydrostatic pressure for embolism reversal in plants of Laurus nobilis [73], we obtain $R \geq 0.24\,\mu$m; then, when all the vessels are tight-filled, germs naturally pre-existing in crude water may spontaneously embolize the tracheids.
Another objection to the confidence in the cohesion-tension theory was also the experiment which demonstrated that tall trees survived double saw-cuts, made through the cross-sectional area of the trunk to sever all xylem elements, by overlapping them [78]. This result, confirmed by several authors does not seem to be in agreement with the possibility of strong negative pressures in the water-tight microtubes [64, 88]. Using a xylem pressure probe, Balling & Zimmermann [3] showed that, in many circumstances, the apparatus does not measure any water tension [98]. However, there are other possibilities for the tree survival and researchers presented some experimental evidences for the local refilling that restores embolized conduits by visualizing the conduits with microscope [11, 12, 53, 67].
A negative argument also seems to come from the crude sap recovery in embolized xylem tubes. At high elevation, it does not seem possible to refill a tube full of air-vapour at a positive pressure when liquid-water is at a negative pressure. In xylem, the liquid-water metastability - due to negative pressures - may persist even in the absence of transpiration. Consequently, refilling processes pose a tough physical challenge to push the liquid-water back into xylem vessels: once embolized vessels have reached a nearly full state, is the refilling solution still at positive pressure with some remaining air?
The most popular theory of refilling process has been proposed in several papers. Due to

the fact that xylem microtubes are generally in contact with numerous living cells [106], it is hypothesized that crude sap is released into the vessel lumen from the adjacent living cells in a manner similar to root exudation [60] and it is assumed that the mechanism for water movement into embolized conduits involves the active secretion of solutes by the living cells [61]. Nonetheless, a survey across species indicated that the root pressure can reach 0.1-0.2 MPa above atmospheric pressure [29] and seems the only logical source of embolized vessels repairing at night in smaller species with well-hydrated soil. The Munch pumping mechanism [71] was invoked, but basic challenges still persist: osmotic pressures measured in sieve tubes do not scale with the height of a plant as one would expect [93] and such scenarios have not yet been empirically verified. Hydraulic isolation is also required to permit the local creation of the positive pressures necessary to force the gas into solution and the embolism removal may be concurrent with tree transpiration [109]. Additively, refilling in the presence of tension in adjacent vessels requires the induction of an energy-dissipating process that locally pumps liquid into the emptied vessels [11] or lowers the water potential in the vessel with the secretion of solutes [111]. As a consequence, many authors suggested that alternative mechanisms must be required [57, 107].

Nowadays, the development of techniques allows us to observe phenomena at length scales of a very few number of nanometers. This nanomechanics reveals new behaviors, often surprising and essentially different from those that are usually observed at macroscopic but also at microscopic scales [8, 33]. As pointed out in experiments, the density of water is found to be changed in narrow pores. The first reliable evidence of this effect was reported by B.V. Derjaguin, V.V. Karasev and E.N. Efremova [23] and found after by many others [24], pp. 240-244. In order to evaluate the structure of thin interlayers of water and other liquids, Green-Kelly and Derjaguin employed a method based on measuring changes in birefringence [50] and they found significant anisotropy of interlayers. Slightly compressible liquids wetting solid substrates point out an unexpected behaviour in which liquids do not transmit the pressure to all their connected domains [26]: it is possible to obtain an equilibrium between connected parts where one is at positive pressure - the pressure in a liquid thin-film - and the other is at negative pressure - the pressure in the liquid bulk. The air-vapour phase in contact with the liquid thin-film is at the same positive pressure as the liquid thin-film. The experiments and model associated with this behaviour fit the disjoining pressure concept [19, 24] which is a well adapted tool for a very thin liquid film of thickness h. In cases of Lifshitz' analysis [26] and van der Waals' theory [100], behaviours of disjoining pressure Π are respectively as $\Pi \sim h^{-3}$ and $\Pi \sim \exp(-h)$. None of them fits experimental results for a film with a thickness ranging over a few nanometers.
Since van der Waals, the fluid inhomogeneities in liquid-vapour interfaces have been represented with continuous models by taking a volume energy depending on space density derivative into account [18, 40, 58, 86, 104]. Nevertheless, the corresponding square-gradient functional is unable to model repulsive force contributions and misses the dominant damped oscillatory packing structure of liquid interlayers near a substrate wall [14, 101]. The decay lengths are correct only close to the liquid-vapour critical point where the damped oscillatory structure is subdominant [27, 28]. In contrast, fluctuations strongly damp oscillatory structure and it is mainly for this reason that van der Waals'

original prediction of a hyperbolic tangent curve in density is so close to simulations and experiments [82].
To propose an analytic expression in density-functional theory for liquid film of a very few nanometer thickness near a solid wall, we add a liquid energy-functional at the solid surface and a surface energy-functional at the liquid-vapour interface to the square-gradient functional representing the volume free energy of the fluid. This kind of functional is well-known in the literature [72] and the process is simpler than the renormalization group theory [30, 36] mainly used near critical points. It was used by Cahn in a phenomenological form [9]. An asymptotic expression is obtained in [41] with an approximation of hard sphere molecules for liquid-liquid and solid-liquid interactions: in this way, we also took account of the power-law behavior which is dominant in a thin liquid film in contact with a solid [55].

The paper is organized as follows: Section 2 expounds that nanofluidic and liquid thin-films concepts are fundamental tools used in the paper; following Derjaguin's Russian school of physical chemistry, we propose an experimental overview of the disjoining pressure concept for liquid thin-films at equilibrium. Section 3 is an analytical and numerical study of the disjoining pressure along vertical liquid thin-films. Section 4 studies the liquid motions along vertical liquid thin-films, and Section 5 is a comparison between liquid-motions' behaviours both in tight-filled microtubes and in liquid thin-films. Section 6 focuses on trees containing vessels considered as machines. From experiments presented in previous sections, a model of xylem using liquid thin-films is proposed. Such a model of xylem allows to explain both the thermodynamical consistence of the cohesion-tension theory and the conditions of the crude-sap refilling at high elevation. This previous *thought experiment* is modified to take account of air-vapour pockets: when the air-vapour pocket pressure is greater than the air-vapour bulk pressure, a huge flow occurs between the two parts filled by air-vapour gas to empty the air-vapour pockets although the liquid-bulk pressure is negative. Finally, the *pancake-layer concept*, associated with the breaking-down of vertical liquid thin-films, allows to forecast the limit of validity of the model and yields a maximum height for the tallest trees.
We present new results concerning models and numerical calculations for comparing filled microtube motions and thin-film motions, a new study of laterally transfer of masses between xylem microtubes and an explanation for ultrasounds eventually generated in the watering network.
A conclusion ends the article. The apparent incompatibility between the model in [44] and the cohesion-tension theory is now solved. Experiments are suggested to verify the accuracy of the sap ascent for tall trees and of the crude-sap's refilling.

2 The disjoining pressure

The disjoining pressure concept is associated with liquid thin-films bordered by vapour bulks and wetting flat solid surfaces. Experiments and analysis are described by Derjaguin *et al* [24]. At given temperature T_0, two experiments allow to understand the physical meaning of horizontal liquid thin-films at equilibrium.

• The first experiment was described in [24] pp. 330–331: a liquid bulk submitted to pressure P_{l_b} contains a microscopic bubble of radius R contiguous to a solid (Fig.

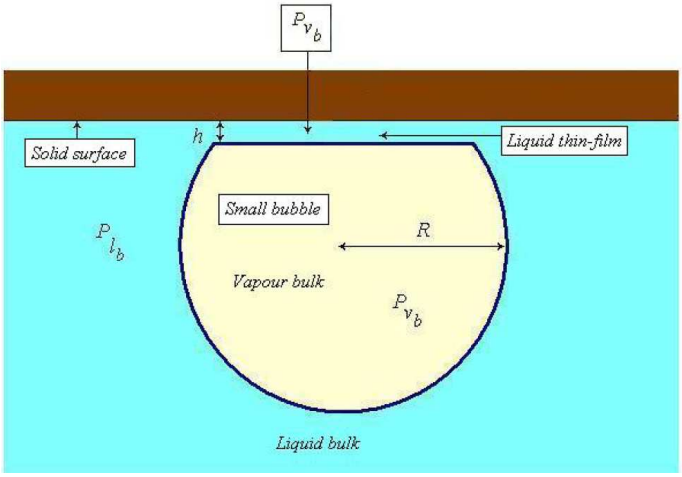

Figure 2: The bubble method of determining the disjoining pressure isotherms of wetting films. The hydrostatic pressure in the liquid thin-film is the same as in the microscopic bubble and is different from the liquid-bulk pressure.

2). The bubble floats upward and approaches a horizontal smooth plate, and a planar liquid thin-film is formed after some time. The liquid thin-film separates the flat part of the bubble which is squeezed onto the solid surface, from inside. Inside the bubble, the pressure of vapour bulk v_b of density ρ_{v_b} (*mother vapour-bulk*) is P_{v_b}. The film is thin enough for gravity to be neglected thickness-wise and the hydrostatic pressure of the liquid thin-film is identical to the vapour-bulk pressure inside the bubble. Pressure P_{v_b} differs from pressure P_{l_b} of liquid bulk l_b of density ρ_{l_b} (*mother liquid-bulk*) [24], page 32. The analysis can apply to the bulk pressure P_{l_b} in the liquid at short distance away from the surface; bulk pressure P_{l_b} is not really affected by the gravity because of the microscopic size of the bubble which remains spherical outside the liquid thin-film. The Young-Laplace formula describes the difference between the two bulk pressures:

$$P_{v_b} - P_{l_b} = \frac{2\gamma}{R}, \tag{1}$$

where γ is the surface tension of the bubble liquid-vapour interface. The liquid thin-film extends from the bulks which create the pressure difference already estimated in Eq. (1) and named $\Pi(h)$:

$$\Pi(h) = P_{v_b} - P_{l_b}\,. \tag{2}$$

Interlayer pressure $\Pi(h)$ additional to the mother liquid-bulk pressure is called the disjoining pressure of the thin film of thickness h, and curve $h \longrightarrow \Pi(h)$ - obtained by changing the bubble's radius and thereby film thickness h - is the *disjoining pressure isotherm*.

• The second experiment is associated with the apparatus due to Sheludko [85] and described in Fig. 3. The film is thin enough such that the gravity effect is neglected across the liquid layer. The hydrostatic pressure in the thin liquid layer included between a solid wall and the vapour bulk differs from the pressure in the contiguous liquid bulk from

which the liquid layer extends (this is the reason for which Derjaguin used mother-bulk term). The forces arising during the thinning of the film of uniform thickness h produce the disjoining pressure which is the additional pressure on the surface of the film to the pressure within the mother liquid-bulk. Clearly, a disjoining pressure could be measured by applying an external pressure to keep the complete layer in equilibrium and verifies Eq. (2).

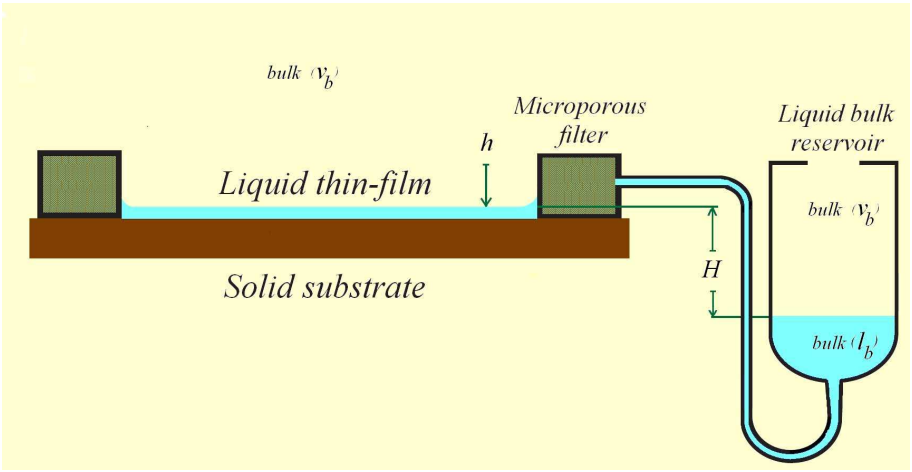

Figure 3: Diagram of the technique for determining the disjoining pressure isotherms of wetting films on a solid substrate: a circular wetting film is formed on a flat substrate to which a microporous filter is clamped. A pipe connects the filter filled with the liquid to a reservoir containing the mother liquid-bulk that can be moved by a micrometric device. Thickness h of the film depends on H in a convenient domain of H-values, where the wetting film is stable. The disjoining pressure is equal to $\Pi = (\rho_b - \rho_{v_b})\,\mathcal{G}\,H$, where $\mathcal{G}$ is the acceleration of gravity ([24], page 332).

Derjaguin's clever idea was to create an analogy between liquid thin-films and liquid-vapour interfaces of bubbles. Liquid thin-films - allowing to obtain an equilibrium between fluid phases at different pressures - are physically similar to *bubbles' flat interfaces*. The pressure in the liquid phase is different from the liquid pressure in the liquid thin-film, which is the same as the pressure in the vapour phase; thereby, the liquid does not completely transmit the pressure in all places where it lays.

Let us consider the Gibbs free energy of the liquid layer (thermodynamic potential). As pointed out by Derjaguin *et al* in ([24], Chapter 2), at temperature T_0, the Gibbs free energy per unit area G can be simply expressed as a function of h:

$$\frac{dG(h)}{dh} = -\Pi(h),$$

and can be integrated as:

$$G(h) = \int_h^{+\infty} \Pi(h)\, dh, \tag{3}$$

where $h = 0$ is associated with the dry wall in contact with the vapour bulk and $h = +\infty$ is associated with a wall in contact with liquid bulk when the value of G is 0.

An important property related to the problem of wetting is associated with the spreading coefficient [21]:

$$S = \gamma_{SV} - \gamma_{SL} - \gamma_{LV},$$

where $\gamma_{SV}, \gamma_{SL}, \gamma_{LV}$ are respectively the solid-vapour, solid-liquid and liquid-vapour free energies per unit area of interfaces. The liquid-layer energy per unit area can be written as

$$E = \gamma_{SL} + \gamma_{LV} + G(h).$$

When $h = 0$, we obtain the energy γ_{SV} of the dry solid wall; when $h = +\infty$, we obtain $\gamma_{SL} + \gamma_{LV}$. In complete wetting of liquid on solid wall, the spreading coefficient is positive.
The conditions of stability of a liquid thin-film essentially depend on phases between which the film is sandwiched. In case of single film in equilibrium between the vapour and a solid substrate, the stability condition is classically:

$$\frac{\partial \Pi(h)}{\partial h} < 0 \quad \Longleftrightarrow \quad \frac{\partial^2 G(h)}{\partial h^2} > 0.$$

The coexistence of two film segments with different thicknesses is a phenomenon which

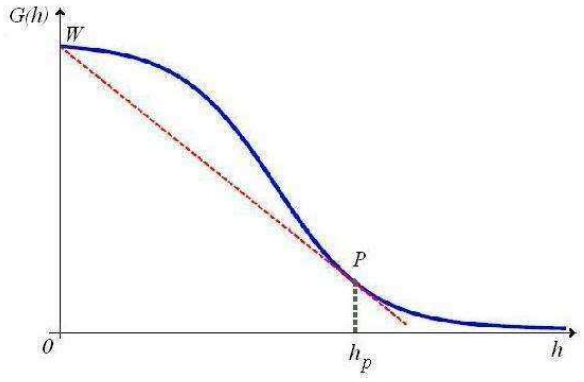

Figure 4: The graph is the sketch of Gibbs free-energy G(h) for liquid water in contact with a wetting solid wall. The construction of the tangent to curve $G(h)$ issued from point W of coordinates $(0, G(0))$ yields point P; point W is associated with a high-energy surface of the dry wall and point P is associated with pancake-thickness h_p [21].

can be interpreted with the equality of chemical potential and superficial tension of the two films. A spectacular case corresponds to the coexistence of a liquid film of thickness h_p and the dry solid wall associated with $h = 0$. The film is the so-called *pancake layer* corresponding to condition

$$G(0) = G(h_p) + h_p \, \Pi(h_p). \tag{4}$$

Equation (4) expresses that the value of the Legendre transformation of $G(h)$ at h_p is equal to $G(0)$. Liquid films of thickness $h > h_p$ are stable and liquid films of thickness $h < h_p$ are metastable or unstable. Thickness h_p can be obtained by the geometric transformation drawn in Fig. 4.

3 Equilibrium of vertical liquid thin-films

3.1 A functional of energy associated with liquid thin-films

The modern understanding of liquid-vapour interfaces begins with papers of van der Waals [75, 100]. In current approaches, it is possible to give exact expressions of the free energy in terms of pair-distribution function and direct correlation function [63]. In practice, these complex expressions must be approximated to lead to a compromise between accuracy and simplicity. When we are confronted with such complications, the mean-field models are generally inadequate and the obtained qualitative picture is no more sufficient. The main alternatives are density-functional theories which are a lot simpler than the Ornstein-Zernike equation in statistical mechanics since the local density is a functional at each point of the fluid [27, 82]. We use this approximation enabling us to analytically compute the density profiles of simple fluids where we take account of surface effects and repulsive forces by adding density-functionals at boundary surfaces. The energy functional of the inhomogeneous fluid in a domain O of boundary ∂O is taken in the form:

$$F_o = \iiint_O \rho\,\varepsilon\; dv + \iint_{\partial O} \varpi\; ds.$$

The first integral is associated with a square-gradient approximation when we introduce a specific free energy ε of the fluid at a given temperature T_0, as a function of density ρ and $\beta = (\operatorname{grad}\rho)^2$ and ϖ is a convenient surface energy. Specific free energy ε characterizes together the fluid properties of compressibility and capillarity. In accordance with kinetic theory,

$$\rho\,\varepsilon = \rho\,\alpha(\rho) + \frac{\lambda}{2}\,(\operatorname{grad}\rho)^2,$$

where term $(\lambda/2)\,(\operatorname{grad}\,\rho)^2$ is added to the volume free-energy $\rho\,\alpha(\rho)$ of the compressible-fluid bulk and coefficient $\lambda = 2\rho\,\varepsilon'_\beta(\rho,\beta)$ (' denotes the partial derivative) is assumed to be constant at given temperature T_0 [81]. Specific free energy α enables to connect continuously liquid and vapour bulks, and thermodynamical pressure $P(\rho) = \rho^2\alpha'_\rho(\rho)$ is a state equation for liquid-vapour interfaces like van der Waals' pressure.
Near a solid wall, London potentials of liquid-liquid and liquid-solid interactions are

$$\begin{cases} \varphi_{ll} = -c_{ll}/r^6\,, & \text{when } r > \sigma_l \text{ and } \quad \varphi_{ll} = \infty \text{ when } \quad r \le \sigma_l\,, \\ \varphi_{ls} = -c_{ls}/r^6\,, & \text{when } r > \delta \text{ and } \quad \varphi_{ls} = \infty \text{ when } \quad r \le \delta\,, \end{cases}$$

where c_{ll} and c_{ls} are two positive constants associated with Hamaker coefficients, σ_l and σ_s denote fluid and solid molecular-diameters, $\delta = \frac{1}{2}(\,\sigma_l + \sigma_s)$ is the minimal distance between centers of fluid and solid molecules [55]. Forces between liquid and solid are short range and can be simply described by adding a special energy at the surface. This

energy is the contribution to the solid/fluid interfacial energy which comes from direct contact. For a plane solid wall at a molecular scale, this surface free energy is in the form:

$$\phi(\rho) = -\gamma_1 \rho + \frac{1}{2}\,\gamma_2\,\rho^2. \tag{5}$$

Here ρ denotes the fluid density value at surface (S); constants γ_1, γ_2 and λ are positive and given by the mean field approximation:

$$\gamma_1 = \frac{\pi c_{ls}}{12\delta^2 m_l m_s}\,\rho_{sol}, \quad \gamma_2 = \frac{\pi c_{ll}}{12\delta^2 m_l^2}, \quad \lambda = \frac{2\pi c_{ll}}{3\sigma_l\, m_l^2},$$

where m_l and m_s denote masses of fluid and solid molecules, ρ_{sol} is the solid density [19, 41].

This is not the entire interfacial energy: another contribution comes from the distortions in the density profile near the wall [9, 19, 41]. We consider a liquid layer contiguous to its vapour bulk and in contact with a plane solid wall (S); the z-axis is perpendicular to the solid surface. The conditions in the vapour bulk are $\operatorname{grad}\rho = 0$ and $\Delta\rho = 0$ where Δ denotes the Laplace operator.

Far below from the fluid critical-point, a way to compute the total free energy of the complete liquid-vapour layer is to add the surface energy of solid wall (S) at $z = 0$, the energy of liquid layer (L) located between $z = 0$ and $z = h$, the energy of the sharp liquid-vapour interface of a few Angström thickness assimilated to surface (Σ) at $z = h$ and the energy of the vapour layer located between $z = h$ and $z = +\infty$ [34]. The liquid at level $z = h$ is situated at a distance order of two molecular diameters from the vapour bulk and the vapour has a negligible density with respect to the liquid density [77].

In our model, the two last energies can be expressed with writing a unique energy ψ per unit surface located on mathematical surface (Σ) at $z = h$: by a calculus like in [41], we can write ψ in the same form than Rel. (5) and expressed in [19] like $\psi(\rho) = -\gamma_5\rho + (1/2)\,\gamma_4\,\rho^2$; but vapour density being negligible, $\gamma_5 \simeq 0$ and surface free energy ψ is reduced to

$$\psi(\rho) = \frac{\gamma_4}{2}\,\rho_h^2, \tag{6}$$

where ρ_h is the liquid density at level $z = h$ and γ_4 is associated with distance d of the order of the fluid molecular diameter (then $d \simeq \delta$ and $\gamma_4 \simeq \gamma_2$).

The properties of Section 2 can be extended to vertical thin-films when we add the gravitational potential Ω to the energy functional; we obtain a functional F in final form

$$F = \iiint_{(L)} \rho\,\varepsilon\; dv + \iiint_{(L)} \rho\,\Omega\; dv + \iint_{(S)} \phi\; ds + \iint_{(\Sigma)} \psi\; ds. \tag{7}$$

In case of equilibrium, functional (7) must be stationary and yields equation of equilibrium and boundary conditions [42, 77, 86].

3.2 Equation of equilibrium

The equation of equilibrium is obtained by using the virtual work principle [35]. We denote by $\delta\boldsymbol{x}$ the variation of Euler position $\boldsymbol{x}$ as defined by Serrin in [87]. For $\delta\mathbf{x}$ null on

the boundaries of L, the integrals on S and Σ have null contributions; the virtual work principle yields:

$$\delta\left(\int_L \rho\,(\varepsilon+\Omega)\,dv\right)=0.$$

Taking into account the relation expressing the variation of a derivative,

$$\delta\left(\frac{\partial\rho}{\partial\boldsymbol{x}}\right)=\frac{\partial\delta\rho}{\partial\boldsymbol{x}}-\frac{\partial\rho}{\partial\boldsymbol{x}}\frac{\partial\delta\boldsymbol{x}}{\partial\boldsymbol{x}},$$

with $\partial/\partial\boldsymbol{x}=\mathrm{grad}^T$, where ^{T} denotes the transposition; we obtain:

$$\delta\beta=2\left(\frac{\partial\delta\rho}{\partial\boldsymbol{x}}-\frac{\partial\rho}{\partial\boldsymbol{x}}\frac{\partial\delta\boldsymbol{x}}{\partial\boldsymbol{x}}\right)\mathrm{grad}\,\rho$$

and

$$\delta\varepsilon=\varepsilon'_\rho\,\delta\rho+\varepsilon'_\beta\,\delta\beta,$$

as well as eqs. (14.5) and (14.6) in [87], then

$$\int_L(-\,\mathrm{div}^T\,\boldsymbol{\sigma}+\rho\,\mathrm{grad}\,\Omega)\,\delta\boldsymbol{x}\,dv=0,$$

where $\boldsymbol{\sigma}=-p\,\mathbf{1}-\lambda\ \mathrm{grad}\,\rho\ \otimes\ \mathrm{grad}\rho$ is the generalization of the stress tensor with $p=\rho^2\varepsilon'_\rho-\rho\ \mathrm{div}\ (\lambda\,\mathrm{grad}\rho)$ [38, 92]. Classical methods of the calculus of variations lead to the equation of equilibrium:

$$\mathrm{div}^T\,\boldsymbol{\sigma}-\rho\ \mathrm{grad}\,\Omega=0.$$

Let us consider an isothermal vertical film of liquid bounded respectively by flat solid wall and vapour bulk; $\boldsymbol{i}$ is the upward direction of coordinate x; then, gravitational potential is $\Omega=\mathcal{G}\,x$, and

$$\mathrm{div}^T\,\boldsymbol{\sigma}-\rho\,\mathcal{G}\,\boldsymbol{i}=0 \tag{8}$$

Coordinate z is normal to the solid wall. Density derivatives are negligible in directions other than z. In liquid-vapour layer (we also call interlayer),

$$\boldsymbol{\sigma}=\begin{bmatrix} a_1, & 0, & 0\\ 0, & a_2, & 0\\ 0, & 0, & a_3\end{bmatrix},\quad\text{with}\quad\begin{cases} a_1=a_2=-P+\dfrac{\lambda}{2}\left(\dfrac{d\rho}{dz}\right)^2+\lambda\,\rho\,\dfrac{d^2\rho}{dz^2}\\[2ex] a_3=-P-\dfrac{\lambda}{2}\left(\dfrac{d\rho}{dz}\right)^2+\lambda\,\rho\,\dfrac{d^2\rho}{dz^2}\end{cases}$$

Equation (8) yields a constant eigenvalue a_3,

$$P+\frac{\lambda}{2}\left(\frac{d\rho}{dz}\right)^2-\lambda\,\rho\,\frac{d^2\rho}{dz^2}=P_{v_{b_x}},$$

where $P_{v_{b_x}}\equiv P(\rho_{v_{b_x}})$ denotes the pressure in vapour bulk v_{b_x} bounding the liquid layer at level x. In the interlayer, eigenvalues a_1, a_2 depend on distance z to the solid wall. In all parts of the isothermal fluid, Eq. (8) can be written [38]:

$$\mathrm{grad}\,(\,\mu-\lambda\,\Delta\rho+\mathcal{G}\,x\,)=0\,, \tag{9}$$

where μ is the chemical potential which is defined to an unknown additive constant. We note that Eqs (8) and (9) are independent of surface energies (5) and (6).
The chemical potential is a function of P and temperature T; due to the equation of state, the chemical potential can be also expressed as a function of ρ and T. We choose as reference chemical potential $\mu_o = \mu_o(\rho)$ which is null for bulks of densities ρ_l and ρ_v associated with the phase equilibrium in normal conditions (temperature T_o and atmospheric pressure P_o [10]). Due to Maxwell's rule, the volume free energy associated with μ_o is $g_o(\rho) - P_o$ where $P_o \equiv P(\rho_l) = P(\rho_v)$ is the bulk pressure and $g_o(\rho) = \int_{\rho_v}^{\rho} \mu_o(\rho)\, d\rho$ is null for the liquid and vapour bulks of the phase equilibrium. Pressure P is [82]:

$$P(\rho) = \rho\, \mu_o(\rho) - g_o(\rho) \ + P_o. \tag{10}$$

Thanks to Eq. (9), we obtain in all the fluid:

$$\mu_o(\rho) - \lambda \Delta\rho + \mathcal{G}\ x = \mu_o(\rho_b),$$

where $\mu_o(\rho_b)$ is the chemical potential value of mother liquid-bulk of density ρ_b such that $\mu_o(\rho_b) = \mu_o(\rho_{v_b})$; ρ_b and ρ_{v_b} are the densities of the mother bulks bounding the layer at level $x = 0$. We emphasize that $P(\rho_b)$ and $P(\rho_{v_b})$ are unequal as drop or bubble bulk pressures. Likewise, we define a mother liquid-bulk of density ρ_{b_x} at level x such that $\mu_o(\rho_{b_x}) = \mu_o(\rho_{v_{b_x}})$ with $P(\rho_{b_x}) \neq P(\rho_{v_{b_x}})$. Then,

$$\lambda\, \Delta\rho = \mu_o(\rho) - \mu_o(\rho_{b_x}) \ \text{ with } \ \mu_o(\rho_{b_x}) = \mu_o(\rho_b) - \mathcal{G}\, x \tag{11}$$

and density derivatives being negligible in directions other than z, in the interlayer,

$$\lambda\, \frac{d^2\rho}{dz^2} = \mu_{b_x}(\rho), \quad \text{with} \quad \mu_{b_x}(\rho) = \mu_o(\rho) - \mu_o(\rho_{b_x}) \tag{12}$$

3.3 Boundary conditions

Condition at solid wall (S) associated with free surface energy (5) yields [42]

$$\lambda \left(\frac{d\rho}{dn}\right)_{|_S} + \phi'(\rho)_{|_S} \ = 0, \tag{13}$$

where n is the external normal direction to the fluid; then, Eq. (13) yields

$$\lambda \left(\frac{d\rho}{dz}\right)_{|_{z=0}} = -\gamma_1 + \gamma_2\ \rho_{|_{z=0}}.$$

The condition at liquid-vapour interface (Σ) associated with the free surface energy (6) yields

$$\lambda \left(\frac{d\rho}{dz}\right)_{|_{z=h}} = -\gamma_4\ \rho_{|_{z=h}}\,. \tag{14}$$

In Eq. (14), density derivative $d\rho/dz$ is large with respect to the variations of the density in the interlayer and corresponds to the drop of density in the liquid-vapour interface. Consequently, Eq. (14) defines the film thickness inside the liquid-vapour interface bordering the liquid layer at surface $z = h$ considered as a dividing-like surface ([82], chapter 3).

3.4 Disjoining pressure of vertical liquid thin-films

Equation (2) can be extended to the disjoining pressure at level x; we obtain the disjoining pressure value:

$$\Pi = P_{v_{b_x}} - P_{b_x}\,,$$

where P_{b_x} and $P_{v_{b_x}}$ are the pressures in mother-liquid and mother-vapour bulks corresponding to level x. At a given temperature T, Π is a function of ρ_{b_x} or equivalently a function of x. Let us denote by

$$g_{b_x}(\rho) = g_o(\rho) - g_o(\rho_{b_x}) - \mu_o(\rho_{b_x})(\rho - \rho_{b_x}), \tag{15}$$

the primitive of $\mu_{b_x}(\rho)$ null for ρ_{b_x}. Consequently, Eq. (10) gives

$$\Pi(\rho_{b_x}) = -g_{b_x}(\rho_{v_{b_x}}), \tag{16}$$

and integration of Eq. (12) yields

$$\frac{\lambda}{2}\left(\frac{d\rho}{dz}\right)^2 = g_{b_x}(\rho) + \Pi(\rho_{b_x}), \tag{17}$$

where $d\rho/dz = 0$ when $\rho = \rho_{v_{b_x}}$.
The reference chemical potential linearized near density ρ_l is $\mu_o(\rho) = (c_l^2/\rho_l)(\rho - \rho_l)$ where velocity c_l is the isothermal sound-velocity in liquid bulk of density ρ_l at temperature T_o [43]. In the liquid part of the liquid-vapour film, Eq. (12) yields:

$$\lambda\frac{d^2\rho}{dz^2} = \frac{c_l^2}{\rho_l}(\rho - \rho_b) + \mathcal{G}\,x \equiv \frac{c_l^2}{\rho_l}(\rho - \rho_{b_x}) \quad \text{with} \quad \rho_{b_x} = \rho_b - \frac{\rho_l}{c_l^2}\,\mathcal{G}\,x. \tag{18}$$

The reference chemical potential linearized near density ρ_v is $\mu_o(\rho) = \dfrac{c_v^2}{\rho_v}(\rho - \rho_v)$ where velocity c_v is the isothermal sound-velocity in vapour bulk of density ρ_v at temperature T_o [43]. In the vapour part of the liquid-vapour film, Eq. (12) yields:

$$\lambda\frac{d^2\rho}{dz^2} = \frac{c_v^2}{\rho_v}(\rho - \rho_{v_b}) + \mathcal{G}\,x \equiv \frac{c_v^2}{\rho_v}(\rho - \rho_{v_{b_x}}) \quad \text{with} \quad \rho_{v_{b_x}} = \rho_{v_b} - \frac{\rho_v}{c_v^2}\,\mathcal{G}\,x.$$

Due to Eq. (11), $\mu_o(\rho)$ has the same value for $\rho_{v_{b_x}}$ and ρ_{b_x}; then

$$\frac{c_l^2}{\rho_l}(\rho_{b_x} - \rho_l) = \mu_o(\rho_{b_x}) = \mu_o(\rho_{v_{b_x}}) = \frac{c_v^2}{\rho_v}(\rho_{v_{b_x}} - \rho_v),$$

$$\text{and} \qquad \rho_{v_{b_x}} = \rho_v\left(1 + \frac{c_l^2}{c_v^2}\frac{(\rho_{b_x} - \rho_l)}{\rho_l}\right).$$

In liquid and vapour parts of the interlayer we have, respectively

$$g_o(\rho) = \frac{c_l^2}{2\rho_l}(\rho - \rho_l)^2 \quad \text{(liquid)} \quad \text{and} \quad g_o(\rho) = \frac{c_v^2}{2\rho_v}(\rho - \rho_v)^2 \quad \text{(vapour)}.$$

From Eqs (15)-(16) we deduce the disjoining pressure at level x:

$$\Pi(\rho_{b_x}) = \frac{c_l^2}{2\rho_l}(\rho_l - \rho_{b_x}) \left[\rho_l + \rho_{b_x} - \rho_v \left(2 + \frac{c_l^2}{c_v^2}\frac{(\rho_{b_x} - \rho_l)}{\rho_l}\right)\right]. \tag{19}$$

Due to $\rho_v \left(2 + \frac{c_l^2}{c_v^2}\frac{(\rho_{b_x} - \rho_l)}{\rho_l}\right) \ll \rho_l + \rho_{b_x}$, we get

$$\Pi(\rho_{b_x}) \approx \frac{c_l^2}{2\rho_l}(\rho_l^2 - \rho_{b_x}^2).$$

At level $x = 0$, the mother liquid-bulk density is closely equal to ρ_l (the density of liquid in phase equilibrium). Due to Eq. (18), Π can be considered as a function of x:

$$\Pi\{x\} \approx \rho_l \, \mathcal{G} \, x \left(1 - \frac{\mathcal{G}\, x}{2\, c_l^2}\right). \tag{20}$$

We denote h_x in place of h for a vertical film, and we consider a film of thickness h_x at level x; the density profile in the liquid part of the liquid-vapour film is solution of system:

$$\begin{cases} \lambda \dfrac{d^2\rho}{dz^2} = \dfrac{c_l^2}{\rho_l}(\rho - \rho_{b_x}), & \text{with boundary conditions :} \\ \lambda \dfrac{d\rho}{dz}_{|_{z=0}} = -\gamma_1 + \gamma_2 \ \rho_{|_{z=0}} \quad \text{and} \quad \lambda \dfrac{d\rho}{dz}_{|_{z=h_x}} = -\gamma_4 \ \rho_{|_{z=h_x}}. \end{cases} \tag{21}$$

Quantities τ and d are

$$\tau \equiv \frac{1}{d} = \frac{c_l}{\sqrt{\lambda \rho_l}} \ ,$$

where d is a reference length; we introduce coefficient $\gamma_3 \equiv \lambda\, \tau$. The solution of System (21) is

$$\rho = \rho_{b_x} + \rho_{1_x}\, e^{-\tau z} + \rho_{2_x}\, e^{\tau z}, \tag{22}$$

where the boundary conditions at $z = 0$ and h_x yield the values of ρ_{1_x} and ρ_{2_x}:

$$\begin{cases} (\gamma_2 + \gamma_3)\rho_{1_x} + (\gamma_2 - \gamma_3)\rho_{2_x} = \gamma_1 - \gamma_2 \rho_{b_x}, \\ -e^{-h_x\tau}(\gamma_3 - \gamma_4)\rho_{1_x} + e^{h_x\tau}(\gamma_3 + \gamma_4)\rho_{2_x} = -\gamma_4 \rho_{b_x}. \end{cases}$$

The liquid density profile is a consequence of solution (22) when $z \in [0, h_x]$. By taking Eq. (22) into account in Eq. (17) and $g_{b_x}(\rho)$ in linearized form in the liquid part of the interlayer, we get

$$\Pi(\rho_{b_x}) = -\frac{2\, c_l^2}{\rho_l}\, \rho_{1_x}\, \rho_{2_x},$$

and consequently,

$$\begin{aligned} \Pi(\rho_{b_x}) \quad = \quad & \frac{2\, c_l^2}{\rho_l} \left[(\gamma_1 - \gamma_2\rho_{b_x})(\gamma_3 + \gamma_4)e^{h_x\tau} + (\gamma_2 - \gamma_3)\gamma_4\rho_{b_x}\right] \times \\ & \frac{\left[(\gamma_2 + \gamma_3)\gamma_4\rho_{b_x} - (\gamma_1 - \gamma_2\rho_{b_x})(\gamma_3 - \gamma_4)e^{-h_x\tau}\right]}{\left[(\gamma_2 + \gamma_3)(\gamma_3 + \gamma_4)e^{h_x\tau} + (\gamma_3 - \gamma_4)(\gamma_2 - \gamma_3)e^{-h_x\tau}\right]^2}. \end{aligned} \tag{23}$$

By identification of expressions (19) and (23), we get a relation between h_x and ρ_{b_x} and a relation between disjoining pressure $\Pi(\rho_{b_x})$ and thickness h_x of the liquid film. For the sake of simplicity, we again finally denote the disjoining pressure by $\Pi(h_x)$ which is a function of h_x at temperature T_o.
Only Eq. (20) depends on $\mathcal{G}$. Due to the fact that Eq. (24) does not depend on $\mathcal{G}$, its expression remains unchanged when we consider h instead of h_x.
Due to $\rho_{b_x} \simeq \rho_b \simeq \rho_l$ [24], the disjoining pressure reduces to the simplified expression

$$\begin{aligned} \Pi(h_x) &= \frac{2\,c_l^2}{\rho_l}\left[(\gamma_1-\gamma_2\rho_l)(\gamma_3+\gamma_4)e^{h_x\tau}+(\gamma_2-\gamma_3)\gamma_4\rho_l\right]\times \\ &\quad \frac{\left[(\gamma_2+\gamma_3)\gamma_4\rho_l-(\gamma_1-\gamma_2\rho_l)(\gamma_3-\gamma_4)e^{-h_x\tau}\right]}{\left[(\gamma_2+\gamma_3)(\gamma_3+\gamma_4)e^{h_x\tau}+(\gamma_3-\gamma_4)(\gamma_2-\gamma_3)e^{-h_x\tau}\right]^2} \\ \text{with} \quad & \Pi(h_x)\equiv\Pi(h). \end{aligned} \tag{24}$$

Let us notice an important property of any fluid mixture consisting of liquid-water, vapour-water and air [39]. The mixture's total-pressure is the sum of the partial pressures of its components, and at equilibrium the partial pressure of air is constant through liquid-air and vapour-air domains. Consequently, results of Section 2 remains unchanged: the disjoining pressure of the mixture is the same as for fluid without air when only a liquid thin-film separates liquid and vapour bulks [46].

3.5 Numerical calculations

Mathematica^{TM} allows us to draw the graphs of $\Pi(h)$ defined by Eq. (24) and $G(h)$ defined by Eq. (3) when $h \in [(1/2)\,\sigma_l, \ell]$, where ℓ is a few tens Ångstroms length. For a few nanometers, the film thickness is not exactly h; we must add an estimated thickness $2\,\sigma_l$ of liquid part of the liquid-vapour interface bordering the liquid layer and the layer thickness is approximatively $h + 2\,\sigma_l$ [82].
We considered water at $T_o = 20°$ C. In S.I. units, experimental values are [47, 55, 62]: $\rho_l = 998\,\mathtt{kg.m^{-3}}$, $c_l = 1.478\times10^3\,\mathtt{m.s^{-1}}$, $c_{ll} = 1.4\times10^{-77}\,\mathtt{kg.m^8.s^{-2}}$, $\sigma_l = 2.8\times10^{-10}\,\mathtt{m}$, $m_l = 2.99\times10^{-26}\,\mathtt{kg}$.
Silica is deposited in many plant tissues such as in bark and wood. We choose $\sigma_s = 2.7\times10^{-10}\,\mathtt{m}$; this value is intermediate between molecular diameter of silicon and diameter of non-spherical molecules of water.
We deduce $\lambda = 1.17\times10^{-16}\,\mathtt{kg^{-1}.m^7.s^{-2}}$, $d = 2.31\times10^{-10}\,\mathtt{m}$, $\gamma_2 = 5.42\times10^{-8}\,\mathtt{kg^{-1}.m^6.s^{-2}}$, $\gamma_3 = 5.06\times10^{-7}\,\mathtt{kg^{-1}.m^6.s^{-2}}$.
The superficial tension of water is $\gamma = 72.5\times10^{-3}\,\mathtt{kg.s^{-2}}$. We choose as Young contact-angle θ between xylem wall and the liquid-water/vapour interface, the arithmetic average of different Young angles propounded in the literature; this value is $\theta = 50$ degrees [65]. Consequently, γ_1 is deduced from the solid-liquid surface energy expressed as $\phi(\rho_s) = -\gamma_1\,\rho_s + (1/2)\,\gamma_2\,\rho_s^2$. Here $\rho_s \simeq \rho_l$ denotes the fluid density value at the surface. The vapour density is negligible with respect to the water-liquid density and Young's relation [82] yields $\gamma\cos\theta = \gamma_1\,\rho_l - (1/2)\,\gamma_2\,\rho_l^2$ and we get $\gamma_1 \approx 75\times10^{-6}\,\mathtt{m^3.s^{-2}}$.
In the upper graph of Fig. 5, we present the free energy graph $G(h_x)$. Due to $h_x > (1/2)\,\sigma_l$, it is not numerically possible to obtain the limit point W corresponding to the dry wall; consequently, point W is obtained by interpolation associated with the concave

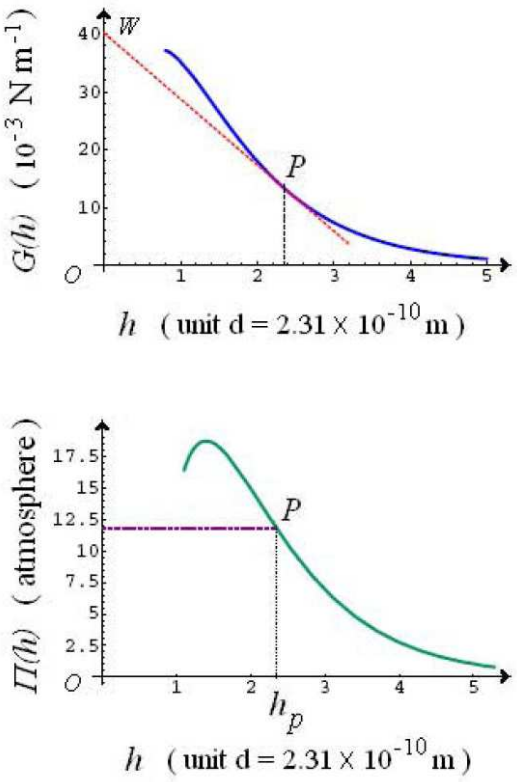

Figure 5: Upper graph: $G(h)$-graph. The unit of $x-$axis graduated by h is $d = 2.31 \times 10^{-10}$ m ; the unit of $y-$axis is 10^{-3} $\mathtt{N}\,\mathtt{m}^{-1}$ (surface tension). Lower graph: $\Pi(h)$-graph. The unit of $x-$axis graduated by h is $d = 2.31 \times 10^{-10}$ m; the unit of $y-$axis is one atmosphere.

part of the G-curve. To obtain pancake thickness h_p corresponding to the smallest thickness of the liquid layer, we draw point P, contact-point of the tangent line issued from W to G-curve. In the lower graph of Fig. 5, we present the disjoining pressure graph $\Pi(h_x)$. The physical part of the disjoining pressure graph corresponding to $\partial\Pi/\partial h_x < 0$ is associated with a liquid layer of several molecules thickness. The non-physical part corresponding to $\partial\Pi/\partial h_x > 0$ is also obtained by Derjaguin *et al* [24] . The reference length d is of the same order as σ_l and is a good length unit for very thin-films. The total pancake thickness is of one nanometer order corresponding to a good thickness value for a high-energy surface [19, 55] ; consequently in the tall trees, at high level, the thickness of the layer is of a few nanometers. The point P of the lower graph corresponds to the point P of upper graph.

4 Dynamics of liquid thin-films along vertical walls

The dynamics of liquid thin-films is studied in the isothermal case. When $h \ll L$, where L is the characteristic length along the wall [45, 76],
i) The velocity component along the wall is large with respect to normal velocity components which can be neglected,
ii) The velocity value varies orthogonally to the wall and it is possible to neglect velocity spatial derivatives along the wall with respect to normal velocity derivatives,
iii) The pressure is constant in the direction normal to the wall. It is possible to neglect inertial term when $Re \ll L/h$, where Re is the Reynolds number of the flow.

The fluid is heterogeneous and the liquid stress tensor is not scalar. However, it is possible to adapt the results obtained for viscous flows to motions in liquid thin-films: due to $\epsilon = h/L \ll 1$, we are in the case of long wave approximation.
We denote the velocity by $\boldsymbol{v} = (u, v, w)$ where (u, v) are the tangential components to the wall. Due to the fact that $e = \sup(|\mathrm{w/u}|, |\mathrm{w/v}|) \ll 1$, we are in the case of lubrication approximation. The main parts of terms associated with second derivatives of liquid velocity components correspond to $\partial^2 u/\partial z^2$ and $\partial^2 v/\partial z^2$.
The density is constant along each stream line ($\dot{\rho} = 0 \Longleftrightarrow div\, \boldsymbol{v} = 0$) and isodensity surfaces contain the trajectories. Then, $\partial u/\partial x, \partial v/\partial y$ and $\partial w/\partial z$ have the same order of magnitude and $\epsilon \sim e$.
As in [81], we assume that the kinematic viscosity coefficient $\nu = \kappa/\rho$, where κ is the dynamic viscosity, only depends on the temperature. In motion equation, the viscosity term is like in liquid bulk [6]

$$(1/\rho)\,\mathrm{div}\ \boldsymbol{\sigma}_v = 2\nu\ [\,\mathrm{div}\ \boldsymbol{D} + \boldsymbol{D}\,\mathrm{grad}\{\,\mathrm{Ln}\,(2\,\kappa)\}\,],$$

where $\boldsymbol{\sigma}_v$ is the viscous stress tensor, $\boldsymbol{D}$ is the velocity deformation tensor and $\boldsymbol{D}$ grad{Ln $(2\,\kappa)$} is negligible with respect to div $\boldsymbol{D}$.
In lubrication and long wave approximations, the liquid nanolayer motion verifies [45, 76]:

$$\boldsymbol{a} + \mathrm{grad}[\,\mu_o(\rho) - \lambda\,\Delta\rho\,] = \nu\,\Delta\boldsymbol{v} - \mathcal{G}\,\boldsymbol{i} \quad \text{with} \quad \Delta\boldsymbol{v} \simeq \left[\,\frac{\partial^2 u}{\partial z^2},\ \frac{\partial^2 v}{\partial z^2}, 0\right],$$

where $\boldsymbol{a}$ denotes the acceleration vector. The equation corresponds to equation of equilibrium (8) with additional inertial-term $\boldsymbol{a}$ and viscous term $\nu\,\Delta\boldsymbol{v}$.
In approximation of lubrication, the inertial term can be neglected [76]:

$$\mathrm{grad}[\,\mu_o(\rho) - \lambda\,\Delta\rho\,] = \nu\,\Delta\boldsymbol{v} - \mathcal{G}\,\boldsymbol{i}. \tag{25}$$

Equation (25) can be separated into tangential and normal components to the solid wall.

- The normal component of Eq. (25) writes in the same form than for equilibrium:

$$\frac{\partial}{\partial z}\,[\,\mu_o(\rho) - \lambda\,\Delta\rho\,] = 0,$$

and consequently,

$$\mu_o(\rho) - \lambda\,\Delta\rho = \mu_o(\rho^*_{b_x}), \tag{26}$$

where $\rho^*_{b_x}$ is the dynamical mother liquid-bulk density at level x (different from ρ_{b_x}, mother liquid-bulk density at level x and at equilibrium, where quantities at equilibrium

have corresponding dynamical quantities indicated by *).
A liquid film of thickness h_x^* is associated to density $\rho_{b_x}^*$. We can write $\mu_o(\rho_b) - \lambda\,\Delta\rho = \eta(h_x^*)$, where function η is such that $\eta(h_x^*) = \mu_o(\rho_{b_x}^*)$.

- For motions colinear to the solid wall and to the gravity (direction $\boldsymbol{i}$ and velocity $u\,\boldsymbol{i}$), by taking account of Eq. (26) the tangential component of Eq. (25) writes:

$$\boldsymbol{i}\,.\,\mathrm{grad}\;\mu_o(\rho_{b_x}^*) = \nu\,\frac{\partial^2 u}{\partial z^2} - \mathcal{G}\,,$$

which is equivalent to

$$\frac{\partial \mu_o(\rho_{b_x}^*)}{\partial \rho_{b_x}^*}\;\frac{\partial \rho_{b_x}^*}{\partial x} = \nu\,\frac{\partial^2 u}{\partial z^2} - \mathcal{G}. \tag{27}$$

Generally, the kinematic condition at solid walls is the adherence condition ($u_{z=0} = 0$). Nevertheless, with water flowing on thin nanolayers [16], there are qualitative observations for slippage when the Young contact angle is not zero [5]. De Gennes said: *the results led us to think about unusual processes which could take place near a wall. They are connected with thickness h of the film when h is of an order of the mean free path* [20]. Recent papers in nonequilibrium molecular dynamics simulations of three dimensional micro Poiseuille flows in Knudsen regime reconsider microchannels: the results point out that the no-slip condition can be observed for Knudsen flow when the surface is rough and the surface wetting condition substantially influences the velocity profiles [91]. In fluid/wall slippage, the condition at solid wall writes:

$$u = L_s \frac{\partial u}{\partial z} \qquad \text{at } z = 0,$$

where L_s is the Navier-length [20]. The Navier-length may be as large as a few microns [91]. At the liquid-vapour interface, we assume that vapour viscosity stress is negligible; from continuity of the fluid tangential-stress through a liquid-vapour interface, we get

$$\frac{\partial u}{\partial z} = 0 \qquad \text{at } z = h_x^*\,.$$

Consequently, Eq. (27) implies

$$\nu\,u = \left(\frac{\partial \mu_o(\rho_{b_x}^*)}{\partial \rho_{b_x}^*}\;\frac{\partial \rho_{b_x}^*}{\partial x} + \mathcal{G}\right)\left(\frac{1}{2}\,z^2 - h_x^*\,z - L_s h_x^*\right).$$

At level x, the mean spatial velocity $\overline{u}$ of the liquid in the nanolayer is

$$\overline{u} = \frac{1}{h_x^*}\int_o^{h_x^*} u\;dz$$

and consequently,

$$\nu\,\overline{\boldsymbol{u}} = -h_x^*\left(\frac{h_x^*}{3} + L_s\right)\;\left[\,\mathrm{grad}\;\mu_o(\rho_{b_x}^*) + \mathcal{G}\,\mathbf{i}\right] \qquad \text{with} \qquad \overline{\boldsymbol{u}} = \overline{\mathrm{u}}\;\boldsymbol{i}\,.$$

Let us note that:

$$\frac{\partial \mu_o(\rho_{b_x}^*)}{\partial x} = \frac{\partial \mu_o(\rho_{b_x}^*)}{\partial \rho_{b_x}^*}\;\frac{\partial \rho_{b_x}^*}{\partial h_x^*}\;\frac{\partial h_x^*}{\partial x} \equiv \frac{1}{\rho_{b_x}^*}\;\frac{\partial P(\rho_{b_x}^*)}{\partial \rho_x^*}\;\frac{\partial \rho_{b_x}^*}{\partial h_x^*}\;\frac{\partial h_x^*}{\partial x}.$$

Due to the fact the vapour-bulk pressure $P^*_{v_{b_x}}$ is constant along the xylem tube, by using relation $\Pi(h^*_x) = P^*_{v_{b_x}} - P^*_{b_x}$, we get along the flow motion

$$\frac{\partial \mu_o(\rho^*_{b_x})}{\partial x} = -\frac{1}{\rho^*_{b_x}} \, \frac{\partial \Pi(h^*_x)}{\partial h^*_x} \, \frac{\partial h^*_x}{\partial x}$$

and consequently,

$$\chi^*_{b_x} \, \overline{\boldsymbol{u}} = h^*_x \left(\frac{h^*_x}{3} + L_s \right) \left[\, \mathrm{grad} \, \Pi(h^*_x) - \rho^*_{b_x} \, \mathcal{G} \, \mathbf{i} \right], \tag{28}$$

where $\chi^*_{b_x} = \rho^*_{b_x} \nu$ is the liquid dynamic-viscosity.
The mean liquid velocity is driven by variation of the disjoining pressure (and film thickness) along the solid wall. Equation (28) differs from classical hydrodynamics; indeed, for a classical liquid thin-films, the Darcy law is $\overline{\boldsymbol{u}} = -K(h) \, \mathrm{grad} \, \wp$, where $\wp$ is the liquid pressure and $K(h)$ is the permeability coefficient. In Eq. (28), the sign is opposite and the liquid pressure is replaced by the disjoining pressure. We note that $\chi^*_{b_x} \simeq \chi$, where χ is the liquid kinetic viscosity in the liquid bulk at phase equilibrium [6]. Moreover $h^*_x / L_s \ll 1$, and slippage is strongly different from the adherence condition corresponding to $L_s = 0$.
The averaged mass equation over the liquid depth is

$$\frac{\partial}{\partial t} \left(\int_0^{h^*_x} \rho \, dz \right) + \mathrm{div} \left(\int_0^{\mathrm{h^*_x}} \rho \, \boldsymbol{u} \, \mathrm{dz} \right) = 0.$$

Since the variation of density is small in the liquid nanolayer, the equation for the free surface is

$$\frac{dh^*_x}{dt} + h^*_x \, \mathrm{div} \, \overline{\boldsymbol{u}} = 0. \tag{29}$$

By replacing (28) into (29) we get

$$\frac{\partial h^*_x}{\partial t} + \frac{1}{\chi} \, \mathrm{div} \left\{ \mathrm{h^{*2}_x} \left(\frac{\mathrm{h^*_x}}{3} + \mathrm{L_s} \right) \left[\, \mathrm{grad} \, \Pi(\mathrm{h^*_x}) - \rho^*_{\mathrm{b_x}} \, \mathcal{G} \, \mathbf{i} \right] \right\} = 0, \tag{30}$$

where $\rho^*_{b_x} \simeq \rho_l$. Equation (30) is a non-linear parabolic equation. If $\partial \Pi(h^*_x)/\partial h^*_x < 0$ the flow is stable. This result is in accordance with the static criterium of stability for liquid thin-films.
When $L_s \neq 0$, we notice the flow is multiplied by the factor $1 + 3L_s/h^*_x$. For example, when $h^*_x = 3 \, \mathtt{nm}$ and $L_s = 100 \, \mathtt{nm}$ which is a Navier length of small magnitude with respect to experiments, the multiplier factor is 10^2; when L_s is $7 \, \boldsymbol{\mu}\mathtt{m}$ as considered in [91], the multiplier factor is 10^4, which seems possible in nanotube observations [48, 65].

In following sections, we use previous tools to study watering of plants and especially trees.

5 The tree watering

5.1 Experiments and analyzes

Since the beginning of the cohesion-tension theory, many efforts have been done to understand crude sap motions and to replicate tree functions when vessels are under tension. Synthetic systems simulating transport processes have played an important role in model testing, and methods creating microfluidic structures to mimic tree vasculature have been developed to capture fundamental aspects of flows and xylem tension [89, 103].

When xylem tubes are completely filled with sap, flows along vessels can be compared with flows through capillaries [106]. Adjacent xylem walls are connected by active bordered-pit membranes with micropores [69]. The membranes separate two volumes of fluid, and generally refer to lipid bilayers that surround living cells or intracellular compartments [90]. The micropores are a few tens of microns wide. Due to the meniscus curvatures at micropore apertures, marking off liquid-water bulk from air-vapour atmosphere, the water-bulk pressure is negative inside micropore reservoirs, but, surprisingly, semi-permeable micropores allow flows of liquid-water at negative pressure to be pushed toward air-vapour domains at positive pressure [96, 97]. Bubbles spontaneously appear from germ existing in crude sap and cavitation makes some tubes embolized [13, 15]. Due to experiments described in Section 2, liquid thin-films must damp embolized xylem walls; consequently, thin-films and microtubes filled of crude sap are in competition.

Optical measurements indicate Young's contact-angles of about 50° for water on the xylem at 20° Celsius [65]. This value suggests that xylem walls are not fully wetting and the capillary spreading cannot really aid the liquid-water refilling but may explain the apparent segregation of liquid-water into droplets [110]. The crude sap is not pure water; its liquid-vapour surface tension has a lower value than the surface tension of pure water and it is possible to obtain the same spreading coefficients with less energetic surfaces.
Water exits the leaves by evaporation through stomata into subsaturated air. Resistance of stomata sits in the path of vapour diffusion between the interior surfaces of leaves and the atmosphere but many of the tallest trees appear to lack active loading mechanisms [32]. When active transpiration occurs, stomata are open and these pumps run. The growth and degrowth of bubbles are rapid within xylem segments, but at night, although the stomata are closed, xylem vessels developing embolies during the day can be refilled with liquid-water and the metastability of the liquid-water may persist even in the absence of transpiration [108, 109].
Recent advances in tree hydraulics have demonstrated that, contrary to what was previously believed, embolism and repair may be far from routine in trees. Trees can recover partially or totally from the deleterious effects of water stress until they reach a lethal threshold of cavitation [22]. This result can be related with the fact that thin films with a thickness greater than the pancake-layer's one are stable and the behaviour is different from bubble stability, which is associated with a saddle point [40].

5.2 Motions in filled microtubes and in thin-films

5.2.1 Generality

One important design requirement is that vapour blockage does not happen in the stems. When the vessel elements are tight-filled with crude sap, liquid motions are Poiseuille

flows [106]. The flow rate through capillary tubes is proportional to the applied pressure gradient, the hydraulic conductivity and depends on the fourth power of capillary radius [2]. To be efficient for sap transportation, the tubes' diameters should be as wide as possible; because of the micron size of the xylem tubes, this is not the case. Consequently, the tracheary elements' network must be important. But the sap movement is induced by transpiration across micropores located in tree leaves and the transpiration is bounded by micropores' sizes; it seems natural to surmise that the diameters of vessels must not be too large to generate a sufficient sap movement.

When the vessel elements are embolized, thin-films damp the xylem walls and Eq. (28) governs the liquid motion. The diameters of capillary vessels which range from 10 to 500 $\boldsymbol{\mu}\mathtt{m}$ and liquid thin-films of some nanometre thickness can be considered as plane interlayers. It is noticeable that trees can avoid having very high energy surfaces: if we replace the flat surfaces of the vessels with corrugated surfaces at molecular scale, it is much easier to obtain the complete wetting requirement, which is otherwise only partial. However, they are still internally wet if crude sap flows through wedge-shaped corrugated pores. The wedge does not have to be perfect on the nanometric scale to significantly enhance the amount of liquid flowing at modest pressures, the walls being endowed with an average surface-energy [17, 102].

It is interesting to compare liquid motions both in tight-filled vessels and liquid-water thin-films. An hydraulic Poiseuille flow is *rigid* due to the liquid incompressibility, the pressure effects are fully propagated in the tube. For a thin layer flow, the flow rate can increase or decrease due to the spatial derivative of h_x^* and depends on the local disjoining pressure. The tree's versatility allows it to adapt to the local disjoining-pressure gradient effects by opening or closing the stomata and the curvature of pit pores, so that the bulk pressure can be more or less negative and the transport of water can be differently dispatched through the stem parts.

5.2.2 Numerical calculations

The treachery network of xylem microtubes is extremely developped. For tree hight $H = 20\,\mathtt{m}$, the total area of xylem walls can be estimated to $S = 30\,\mathtt{km}^2 \equiv 3\times10^7\,\mathtt{m}^2$ [106]. We consider xylem microtubes with diameter $2R = 50\,\boldsymbol{\mu}\mathtt{m} \equiv 5\times10^{-5}\mathtt{m}$. The dynamic viscosity of liquid water at 20° Celsius is $\chi = 10^{-3}\,\mathtt{kg.m}^{-1}\mathtt{.s}^{-1}$. It is experimentally verified that in tightly-filled microtubes, the crude sap velocity usually goes from $1\,\mathtt{m.hour}^{-1} \equiv 2.8\times10^{-4}\mathtt{m.s}^{-1}$ to $100\,\mathtt{m.hour}^{-1} \equiv 2.8\times10^{-2}\mathtt{m.s}^{-1}$ in maximal transpiration [105]. The mean velocity of Poiseuille's flows verifies

$$\overline{u}_1 = \frac{R^2}{8\chi}\ \left|\mathrm{grad}\ \left(-\wp_{b_x^*}\right)\right|,$$

where $\wp_{b_x^*}$ is the liquid pressure at level x. Consequently, $\left|\mathrm{grad}\ \left(-\wp_{b_x^*}\right)\right|$ goes from 3.6×10^{-2} $\mathtt{atmosphere.m}^{-1} \equiv 3.6\times10^3\,\mathtt{Pa.m}^{-1}$ to 3.6 $\mathtt{atmosphere.m}^{-1} \equiv 3.6\times10^5\,\mathtt{Pa.m}^{-1}$. The number of xylem microtubes can be calculated as $N = S/(2\,\pi\,R\,H)$; we approximatively obtain $N = 10^{10}$ microtubes and the total flow is

$$Q_1 = N\frac{\pi R^4}{8\,\chi}\ \left|\mathrm{grad}\ \left(-\wp_{b_x^*}\right)\right|.$$

For a velocity $\overline{u}_1 = 1\,\mathtt{m.hour}^{-1} \equiv 2.8{\times}10^{-4}\,\mathtt{m.s}^{-1}$, $Q_1 = 5.5{\times}10^{-3}\mathtt{m}^3\mathtt{.s}^{-1} \equiv 5.5\,\mathtt{liters/s}$ and for $\overline{u}_1 = 100\,\mathtt{m.hour}^{-1} \equiv 2.8 \times 10^{-2}\,\mathtt{m.s}^{-1}$, $Q_1 = 5.5 \times 10^{-1}\,\mathtt{m}^3\mathtt{.s}^{-1} \equiv 550\,\mathtt{liters/s}$ corresponding to values of biological experiments.
In embolized microtubes, mean velocity u_2 along thin-films is given by Rel (28). Pressure $P_{v_{b_x}} \approx P_v$ being constant and $\rho^*_{b_x} \approx \rho_l$, then

$$\mathrm{grad}\left(\Pi(h^*_x) - \rho^*_{b_x}\,\mathcal{G}\,x\right) \approx \mathrm{grad}\left(-P_{b^*_x} - \rho_l\,\mathcal{G}\,x\right).$$

From $\chi\,\overline{u}_2 \approx h_x L_s\,\left|\mathrm{grad}\left(\Pi(h^*_x) - \rho_{b^*_x}\,\mathcal{G}\,x\right)\right|$, together with a layer thickness $h_x = 10\,\mathtt{nm} \equiv 10^{-8}\,\mathtt{m}$, $L_s = 7\,\boldsymbol{\mu}\mathtt{m} \equiv 7 \times 10^{-6}\,\mathtt{m}$, and $\left|\mathrm{grad}\left(\Pi(h^*_x) - \rho_{b^*_x}\,\mathcal{G}\,x\right)\right| = 3.6 \times 10^5\ \mathtt{Pa.m}^{-1}$, we obtain $\overline{u}_2 = 2.5{\times}10^{-5}\,\mathtt{m.s}^{-1}$ which is 11 times less than velocity in tight-filled microtubes for a velocity of $1\ \mathtt{m.hour}^{-1}\,\mathtt{m} \equiv 2.8 \times 10^{-4}\mathtt{m.s}^{-1}$.
For N microtubes, the total flow is

$$Q_2 = N2\pi R h_x u_2$$

and for 10^{10} microtubes, $Q_2 = 4 \times 10^{-7}\,\mathtt{m}^3\mathtt{.s}^{-1} \equiv 0.4\,\mathtt{cm}^3\mathtt{.s}^{-1}$ which is very small with respect to the sum of Poiseuille's flows.
It seems that the liquid thin-films do not affect the watering of trees but in next Section 6, we see it is not the case. For an ascent of $50\,\mathtt{m}$, we obtain an ascent time of $2 \times 10^6\,\mathtt{s} \equiv 23$ days which estimates the tree-recovery time in spring.

6 Embolization and recovery

6.1 A diagram of vessel elements for tall trees

In physical conditions of Subsection 3.4 and temperature at 20° Celsius, we consider two vertical adjacent vessels linked by micropore reservoirs with pit membranes dotting their walls. The bordered-pit membranes are of the order of few tens of microns corresponding to the microporous filters in Fig. 6. The mother vapour-bulk contains air and the mother liquid-water bulk also contains dissolved air.
One vessel - corresponding to subsaturated mother air-vapour bulk - is embolized with a positive pressure; it generates a liquid thin-film which wets the xylem wall. The other vessel is filled with the mother liquid-water bulk at a negative pressure linked to the liquid thin-film thanks to a micropore reservoir with a bordered-pit membrane.

Such a system can be in equilibrium, although the pressure is not the same in the two adjacent vessels.
In the same configuration, the vessel elements are now assumed to be weakly out-of-equilibrium. As explained in Section 4, the driving force of the sap ascent comes from the decreasing thickness of the liquid thin-film wetting the walls in the embolized vessels; consequently the negative pressure value of the mother liquid-water bulk in micropore reservoirs decreases (its absolute value increases). Additionally, air-vapour pockets can coexist with the mother liquid-water bulk of one of the two vessels. The air-vapour pockets also generate liquid thin-films bordering xylem walls (see Fig. 7).
Due to their curvature, the pressures of air-vapour pockets are generally higher than the mother vapour-bulk pressure in the other vessel. The vapour pockets and their liquid thin-films empty into the vessel with the lower air-vapour bulk pressure. The analogy

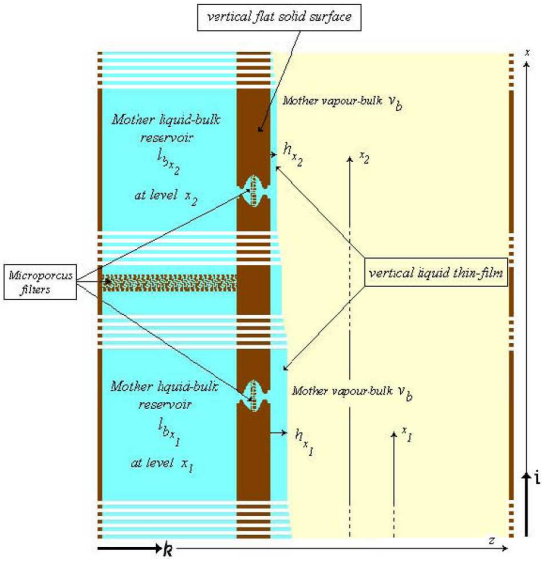

Figure 6: Diagram of a vertical liquid thin-film. A liquid thin-film bordered by a mother vapour-bulk (v_b) wets a vertical flat solid surface. Mother liquid-bulk (l_{b_x}), but not mother vapour-bulk (v_b), depends on the x-level. Like on Sheludko's apparatus, microporous filters connect the mother liquid-bulk reservoir at different altitudes with the liquid thin-film. Different parts of the mother liquid-bulk reservoir can also be connected by microporous filters.

proposed in Section 2 between liquid thin-films and liquid-vapour interfaces of bubbles allows to simply understand the directions of motions between air-vapour pockets and the mother air-vapour bulk: for example, when two bubbles are included in a liquid bulk (corresponding to the mother liquid-water bulk at negative pressure), the smallest bubble with the greatest pressure (i.e. the air-vapour pocket) empties into the largest bubble with the lowest pressure (i.e. the air-vapour bulk of the embolized vessel) [66].
Such events happen in particular at night, when - due to the absence of evaporation - the vapour is subsaturated in embolized vessels; the curvature of the air-vapour pockets generates a pressure greater than the pressure in the embolized vessels. Conversely, during the day and strong sunlight, the vapour in vessels is saturated by evaporation; the air-vapour pressure increases in the embolized vessels and the air-vapour gas must flow back into the vessels with air-vapour pockets of subsaturated vapour included in the mother liquid-water bulk at negative pressure.
It is not surprising that the heartwood may contain liquid under positive pressure while in the sapwood the transpiration stream moves along a gradient of negative pressure. Embolized vessels creating thin-films may provide a key contribution to tree refilling. Crude sap in the heartwood can also fill the vessel elements at negative pressure through the bordered-pit membranes. Consequently, embolized microtubes of xylem fundamentally contribute to the crude-sap ascent and to the refilling of the tree as machine allowing to obtain equilibrium between fluid phases at different pressures and consequently to recover the water from cavitation.

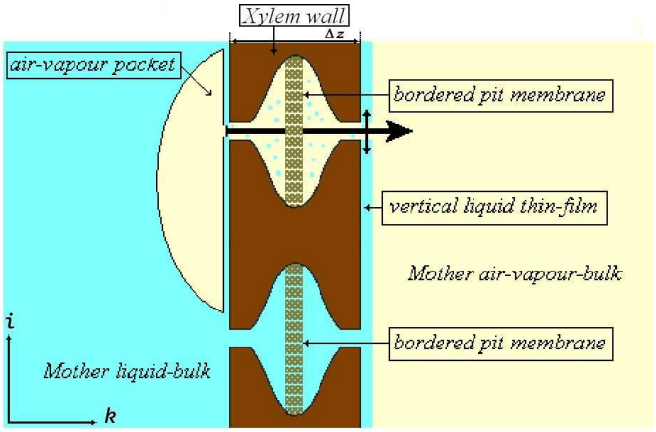

Figure 7: At equilibrium between bulks at altitude x, mother liquid-bulk (l_{b_x}) balances the liquid thin-film and mother air-vapour-bulk (v_b). It is not true for the vapour pocket and the mother air-vapour-bulk: when the pressure in the air-vapour pocket is greater than the pressure in mother air-vapour-bulk, the air-vapour pocket empties into the mother air-vapour-bulk.

6.2 Numerical values of the mass transfer

It is interesting to estimate the magnitude of air-vapour flows between air-vapour pockets and the mother air-vapour bulk. At altitude x, the mother bulks are still named (l_{b_x}) and (v_b), respectively. At equilibrium between the two mother bulks, the vertical liquid thin-film between the mother air-vapour bulk and the xylem wall is also at equilibrium and at the same pressure as the mother air-vapour bulk. Depending on reservoir altitude x, the mother liquid-bulk can be at negative pressure.

The channels crossing from the left to the right parts of the xylem wall can be considered as sound pipes (Fig. 7). We denote by e and $2r$ the length and diameter of pipes, respectively. The pipe diameters are assumed to be of the same order than diameters of pits bordering the xylem walls. The difference of pressure between air-vapour pockets and the mother air-vapour bulk is denoted by $\triangle P$. The flow is assumed to be Poiseuille flow and the mean velocity along the channel is [2]:

$$\overline{v} = \frac{r^2}{8\chi}\,\frac{\triangle P}{e}. \tag{31}$$

The velocity is null in the mother air-vapour bulk and in the air-vapour pockets creating a velocity-pulse between the two extremities of the pipe.

On one hand, we assume that the pressure in the air-vapour pocket is greater than the pressure in the mother air-vapour bulk. The air-vapour pocket and the mother air-vapour bulk are not at equilibrium. The liquid thin-film between the air-vapour pocket and the xylem wall is thinner than the liquid thin-film between the mother air-vapour bulk and the xylem wall (see Fig. 7).
We consider experimental values:
$e = 50\,\mu\mathtt{m} \equiv 5 \times 10^{-5}\,\mathtt{m}$, $r = 10\,\mu\mathtt{m} \equiv 1 \times 10^{-5}\,\mathtt{m}$, $\chi = 1.81 \times 10^{-5}\,\mathtt{kg.m^{-1}.s^{-1}}$ for air-vapour viscosity and the saturated vapour pressure of water is $2.3 \times 10^{-2}\,\mathtt{atmosphere} \equiv$

$2.3 \times 10^3\,\mathtt{Pa}$ at 20° Celsius [62, 106]. In the case of a difference of pressure between the saturated vapour pressure in air-vapour pocket and the sub-saturated vapour pressure in the mother air-vapour bulk $\triangle P = 10^{-2}\,\mathtt{atmosphere} \equiv 10^3\,\mathtt{Pa}$, we obtain $\overline{v} = 14\,\mathtt{m.s}^{-1}$ and the crossing time of the pipe is $\tau = e/\overline{v} = 3.6 \times 10^{-6}\,\mathtt{s}$ corresponding to a pulse frequency $\omega = \tau^{-1} \approx 2.8 \times 10^5\,\mathtt{Hz} \equiv 280\,\mathtt{KHz}$ associated with ultrasonic vibrations.
It is interesting to calcutate the flow through the pipe,

$$q = \frac{\pi r^4}{8\,\chi}\,\frac{\triangle P}{e}.$$

We obtain $q = 4.3 \times 10^{-9}\,\mathtt{m}^3.s^{-1} \equiv 4.3 \times 10^{-3}\,\mathtt{cm}^3.s^{-1}$.
Conversely, when the mother air-vapour pressure is slightly greater than the air-vapour pocket pressure, the air-vapour bulk can embolize the liquid tight-filled vessel elements with opposite velocity and consequently the same pulse frequency for the same difference of pressure between mother air-vapour-bulk and air-vapour pockets.
Let us note that the saturated vapour pressure quickly decreases with the temperature. At 0° Celsius, the saturated vapour pressure of water is $6 \times 10^{-4}\,\mathtt{atmosphere} \equiv 60\,Pa$ and $\triangle P$ drastically decreases as the flow through the pipe, and it may be a reason of embolization at low temperature.

On the other hand, the crude sap in the tight-filled microtubes can spread in the embolized microtubes when the disjoining pressure is smaller than the disjoining pressure at equilibrium. Equation (31) allows to calculate the mean velocity of the flow: here $\triangle P$ represents the difference between the disjoining pressure values at and out from equilibrium.
With $\triangle P = 10^{-1}\,\mathtt{atmosphere} \equiv 10^4\,\mathtt{Pa}$ and $\chi = 10^{-3}\,\mathtt{kg.m}^{-1}$, we obtain $\overline{v} = 2.5\,\mathtt{m.s}^{-1}$ and the crossing time of the pipe is $\tau = e/\overline{v} = 2 \times 10^{-5}\,\mathtt{s}$ corresponding to a pulse frequency $\omega = \tau^{-1} \approx 5 \times 10^4\,\mathtt{Hz} \equiv 50\,\mathtt{KHz}$. We also obtain $q = 0.8 \times 10^{-9}\,\mathtt{m}^3.s^{-1} \equiv 0.8 \times 10^{-3}\,\mathtt{cm}^3.s^{-1}$.

Due to the size of xylem microtubes, a reference diameter of bubbles can be about $2R = 50\,\boldsymbol{\mu}\mathtt{m} \equiv 5 \times 10^{-5}\,\mathtt{m}$ corresponding to volume $V = 6.5 \times 10^{-14}\,\mathtt{m}^3 \equiv 6.5 \times 10^{-8}\,\mathtt{cm}^3$ and for both liquid and gas exchanges, the transfers of masses are extremely fast.

The fast accelerations of air-vapour gas through micropores generate ultrasounds associated with pulse frequencies and may explain the acoustical measurements obtained in experiments [70, 94].

The magnitude of the viscosity of simple wetting fluids increases when they are confined between solid walls, and there is a direct correlation between the air-seeding threshold and the pit pore membranes' diameters [56]. However, the acceleration magnitude is so large that it remains very important for viscous fluids and semi-permeable bordered-pit membranes.

6.3 Limit of the disjoining pressure model and topmost trees

Liquid thin-films primarily contribute to xylem microtubes refilling and consequently the refilling is not possible when the liquid thin-films break down. Amazingly, the above study allows to estimate a maximum of thin-films' altitude. In Subsection 3.5 and in

Fig. 5, we have seen that the thickness of the liquid thin-film decreases when its altitude increases and the liquid thin-film disrupts when thickness reaches the pancake layer thickness-value.

The pancake layer of thin-films was presented in Section 2 and a numerical simulation associated with experimental data of xylem at temperature 20° Celsius is presented in Subsection 3.5. As indicated in Subsection 3.5, the Young contact angle between a xylem wall and a liquid-vapour water interface is $\theta \approx 50°$.

The upper graph in Fig. 5 presents the free energy $G(h)$ associated with physical values of trees' xylem walls. The lower graph of Fig. 5, presents the disjoining pressure $\Pi(h)$ and is in accordance with experimental curves obtained in the literature [24, 44]. The total pancake thickness h_p is about one nanometer order corresponding to a good thickness value for a high-energy surface [19]; consequently in tall trees, at high level, the thickness of the liquid thin-film must be of a few nanometers. Point P on the lower graph corresponds to point P on upper graph. When $x_{_P}$ corresponds to the altitude of the pancake layer, Eq. (20) and $\mathcal{G}x/(2\,c_l^2) \ll 1$ yields $\Pi(h_p) \simeq \rho_l\,\mathcal{G}\,x_{_P}$. From the lower graph in Fig. 5, we obtain a maximum thin-film height of 120 meters corresponding to 12 atmospheres. At this altitude, we must approximatively add 20 meters corresponding to the ascent of sap due to capillarity and osmotic pressure [10, 83] and we obtain 140 meters. This level corresponds to the level order of the topmost trees, as a giant, 128 meter-tall eucalyptus or a 135 meter-tall sequoia which were reported in the past by Flindt [31].

Other mechanical or biological constraints may suggest adaptation to height-induced costs [59], but nevertheless our model limits the maximum height of trees. The tallest trees are not the ones with the largest demand for tension; it is rather dry climate shrubs that demand it [4]. This observation seems to be in accordance with the possible existence of thin-films in embolized vessels at high elevation.

7 Conclusion

In the trees, xylem microtubes are naturally filled with sap up to an altitude of a few ten meters. Above this altitude, when xylem tubes can be embolized, the molecular forces create crude sap thin-films along the walls of xylem associated with micropore pressures versatilely adapted thanks to pit membranes. The disjoining pressure of liquid thin-films is the exhaust valve filling the xylem microtubes and allowing crude sap to ascend. Consequently, the embolized vessels constitute a necessary network for the watering and the recovery of tall trees (Lampinen and Noponen argued that embolisms were necessary for the ascent of sap [61]). The model explains aspects of sap movement which the classical cohesion-tension theory was hitherto unable to satisfactorily account for, e.g. the refilling of the vessels in spring, in the morning or after embolism events, as well as the compatibility with thermodynamics' principles. Nevertheless, the xylem tight-filled microtubes under tension are the essential network of tree watering.

Simple in vivo observations at the nanometre thickness of liquid thin-films are not easy to implement and the direct measurement difficulties prevent their detection. The progression of MEMS technology [91], and tomography [52], may provide a new route towards this goal. If these biophysical considerations are experimentally verified, they would prove that trees can be an example to use technologies for liquids under tension connected with liquids in contact with solid substrates at nanoscale range. They would provide a con-

text in which nanofluid mechanics points to a rich array of biological physics and future technical challenges.
It is wondering to observe that the density-functional theory expressed by a rough energetic model with a surface density-functional at the walls enables to obtain a good order of the ascent of sap magnitude. The result is obtained without too complex weighted density-functional and without taking account of quantum effects corresponding to less than an Amgström length scale. These observations seem to prove that this kind of functionals can be a good tool to study models of liquids in contact with solids at a small nanoscale range.
Moreover there exists no conflict between thermodynamics and cohesion-tension theory [37, 38].

Acknowledgements: *H.G. thanks the Accademia Nazionale dei Lincei, the Istituto Nazionale di Alta Matematica F. Severi (INdAM), and the Gruppo Nazionale per la Fisica Matematica (GNFM), for their nice invitation and support to the conference on "New Frontiers in Continuum Mechanics" hold at the Academy on 21 and 22 June 2016.*

References

[1] Askenasy E., *Ueber das Saftsteigen*. Verh. Nat. Med. Ver. Heidelb. 5 (1895) 325–345.

[2] Batchelor G.K., *An Introduction to Fluid Dynamics*. Cambridge U. Press (1967).

[3] Balling A. - Zimmermann U., *Comparative measurements of the xylem pressure of nicotiana plants by means of the pressure bomb and pressure probe*. Planta, 182 (1990) 325–338.

[4] Benkert R. - Balling A. - Zimmermann U., *Direct measurements of the pressure and flow in the xylem vessels of nicotiana tabacum and their dependence on flow resistance and transpiration rate*. Botanica Acta, 104 (1991) 423–432.

[5] Blake T., *Slip between a liquid and a solid: D.M. Tolstoi's (1952) theory reconsidered*. Colloids Surf., 47 (1990) 135–145.

[6] Bocquet L. - Charlaix E., *Nanofluidics, from bulk to interfaces*. Chem. Soc. Rev., 39 (2010) 1073–1095.

[7] Boehm J., *Capillarität und Saftsteigen*. Ber. Deut. Botan. Ges., 11 (1983) 203–212.

[8] Bhushan B., *Springer Handbook of Nanotechnology*. Springer, Berlin (2004).

[9] Cahn J.W., *Critical point wetting*. J. Chem. Phys., 66 (1977) 3667–3672.

[10] Callen H.B., *Thermodynamics and an Introduction to Thermostatistics*. 2nd ed., Wiley, New York (1985).

[11] Canny M.J., *Vessel contents during transpiration - embolisms and refilling*. American Journal of Botany, 84 (1997) 1223–1230.

[12] Canny M.J., *Embolism and refilling in the maize leaf lamina and the role of the protoxylem lacuna*. American Journal of Botany, 88 (2001) 47-51.

[13] Canny M.J. -Sparks J.P. -Huang C.X. - Roderick M.L., *Air embolisms exsolving in the transpiration water - the effect of constrictions in the xylem pipes*. Functional Plant Biology, 34 (2007) 95–111.

[14] Chernov A.A. - Mikheev L.V., *Wetting and surface melting: Capillary fluctuations versus layerwise short-range order*. Physica A, 157 (1989) 1042–1058.

[15] Choat B. - Cobb A. - Jansen S., *Structure and function of bordered pits: New discoveries and impacts on whole plant hydraulic function*. New Phytologist, 177 (2008) 608-626.

[16] Churaev N.V., *Thin liquid layers*. Colloid Journal, 58 (1996) 681–693.

[17] Concus P. - Finn R., *On the behavior of a capillary surface in a wedge*. Proc. Nat. Acad. Sci., 63 (1969) 292–299.

[18] dell'Isola F. - Gouin H. - Rotoli G., *Nucleation of spherical shell-like interfaces by second gradient theory: numerical simulations*. Eur. J. Mech., B/Fluids, 15 (1996) 545–568.

[19] de Gennes P.G., *Wetting: statics and dynamics*. Review of Modern Physics, 57 (1985) 827-863.

[20] de Gennes P.G., *On the fluid/wall slippage*. Langmuir, 8 (2002) 3413–3414.

[21] de Gennes P.G. - Brochard-Wyart F. - Quéré D., *Capillarity and Wetting Phenomena: Drops, Bubbles, Pearls, Waves*. Springer, New York (2004).

[22] Delzon S. - Cochard H., *Recent advances in tree hydraulics highlight the ecological significance of the hydraulic safety margin*. New Phytologist 203 (2014) 355–358.

[23] Derjaguin B.V. - Karasev V.V. - Efremova E.N., *Thermal expansion of water in fine pores*. J. Colloid Interface Sci., 109 (1986) 586–587.

[24] Derjaguin B.V. - Churaev N.V. - Muller V.M., *Surface Forces*, originally published by Plenum Publishing Corporation and re-edited by Springer Science+Business Media (1987).

[25] Dixon H.H. - Joly J., *On the ascent of sap*. Philosophical Transactions of the Royal Society of London B, 186 (1894) 563–576.

[26] Dzyaloshinsky I.E. - Lifshitz E.M. - Pitaevsky L.P., *The general theory of van der Waals forces*. Advance in Physics, 10 (1961) 165–209.

[27] Evans R., *The nature of liquid-vapour interface and other topics in the statistical mechanics of non-uniform classical fluids*. Adv. Phys., 28 (1979) 143–200.

[28] Evans R. - Leote de Carvalho J.F. - Henderson J.R. - Hoyle D.C., *Asymptotic decay of correlations in liquids and their mixtures*. J. Chem. Phys., 100 (1994) 591–603.

[29] Fisher J.B. - Angeles G. - Ewers F.W. - Lopez-Portillo J., *Survey of root pressure in tropical vines and woody species*. International Journal of Plant Sciences, 158 (1997) 44-50.

[30] Fisher M.E. - Jin A.J., *Effective potentials, constraints, and critical wetting theory*. Phys. Rev. B, 44 (1991) 1430–1433.

[31] Flindt R., *Amazing Numbers in Biology*. Springer, New York (2006).

[32] Fu Q.S. - Cheng L.L. - Guo Y.D. - Turgeon R., *Phloem loading strategies and water relations in trees and herbaceous plants*. Plant Physiology, 157 (2011) 1518-1527.

[33] Gărăjeu M. - Gouin H. - Saccomandi G., *Scaling Navier-Stokes equation in nanotubes*. Physics of fluids, 25 (2013) 082003 & arXiv:1311.2484.

[34] Gavrilyuk S.L. - Akhatov I., *Model of a liquid nanofilm on a solid substrate based on the van der Waals concept of capillarity*, Phys. Rev. E., 73 (2006) 021604.

[35] Germain P., La méthode des puissances virtuelles en mécanique des milieux continus, Journal de Mécanique, 12 (1973) 236–274.

[36] Goldenfeld N., *Lectures on phase transitions and the renormalization group*. Addison-Wesley, Boston (1993).

[37] Gouin H., *Thermodynamics form of the equation of motion for perfect fluids*. Comptes Rendus de l'Académie des Sciences de Paris, 305 II (1987) 833–838 & arXiv:1006.0802.

[38] Gouin H., *Utilization of the second gradient theory in continuum mechanics to study the motion and thermodynamics of liquid-vapour interfaces*, Physicochemical Hydrodynamics B: Physics Vol. 174, Plenum Publ. Corp., New York (1988) 667–682 & arXiv:1108.2766

[39] Gouin H., *Variational theory of mixtures in continuum mechanics*. Eur. J. Mech, B/Fluids (1990) 469–491 & arXiv:0807.4519.

[40] Gouin H. - Slemrod M., *Stability of spherical isothermal liquid-vapour interfaces*. Meccanica, 30 (1995) 305–319.

[41] Gouin H., *Energy of interaction between solid surfaces and liquids*. The Journal of Physical Chemistry B, 102 (1998) 1212–1218 & arXiv:0801.4481

[42] Gouin H. - Kosiński W., *Boundary conditions for a capillary fluid in contact with a wall.* Arch. Mech. 50 (1998) 907–916 & arXiv:0802.1995

[43] Gouin H. - Espanet L., *Bubble number in a caviting flow.* Comptes Rendus Acad. Sci. Paris, 328 IIb (2000) 151–157 & arXiv:0807.5023

[44] Gouin H., *A new approach for the limit to tree height using a liquid nanolayer model.* Continuum Mechanics and Thermodynamics 20 (2008) 317–329 & arXiv:0809.3529

[45] Gouin H. - Gavrilyuk S., *Dynamics of liquid nanofilms.* International Journal of Engineering Science, 46 (2008) 1195–1202 & arXiv:0809.3489

[46] Gouin H., *Liquid Nanofilms. A mechanical model for the disjoining pressure.* International Journal of Engineering Science, 47 (2009) 691–699 & arXiv:0904.1809

[47] Gouin H., *Solid-liquid interaction at nanoscale and its application in vegetal biology.* Colloids and Surfaces A, 383 (2011) 17–22 & arXiv:1106.1275

[48] Gouin H., *Statics and dynamics of fluids in nanotubes.* Note di Matematica, 32 (2012) 105–124 & arXiv:1311.2303.

[49] Gouin H., *The watering of tall trees - Embolization and recovery*, Journal of Theoretical Biology, 369 (2015) 42–50 & arXiv:1404.4343

[50] Green-Kelly D. - Derjaguin B.V., *Research in Surfaces Forces*, vol. 2, Consultants Bureau, New York (1966) p. 117.

[51] Herbert E. - Caupin F., *The limit of metastability of water under tension: theories and experiments.* J. Phys. Condens. Matter, 17 (2005) S3597-S3602.

[52] Herman G.T., *Fundamental of Computarized Tomography: Image Reconstruction from Projection.* Springer, New York, 2nd Edition (2009).

[53] Holbrook N.M. - Zwieniecki M.A., *Embolism repair and xylem tension: do we need a miracle?* Plant Physiology, 120 (1999) 7–10.

[54] Holbrook N.M. - Zwieniecki M.A., Eds., *Vascular Transport in Plants.* Elsevier, Amsterdam (2005).

[55] Israelachvili J., *Intermolecular Forces.* Academic Press, New York (1992).

[56] Jansen S. - Choat B. - Pletsers A., *Morphological variation of intervessel pit membranes and implications to xylem function in angiosperms.* American Journal of Botany, 96 (2009) 409–419.

[57] Johnson R.J. - Canny M.J., *Phloem translocation of organic compounds: a possible mechanism to assist osmotically-generated pressure flow in tall trees.* Water, 4 (2013) 112–128.

[58] Kazmierczak B. - Piechór K., *Parametric dependence of phase boundary solution to model kinetic equations.* ZAMP 53 (2002) 539–568.

[59] Koch W. - Sillett S.C. - Jennings G.M. - Davis S.D., *The limit to tree height.* Nature, 428 (2004) 851–854.

[60] Kramer P.J. - Boyer J.S., *Water Relations of Plants and Soils.* Academic Press, San Diego (1995).

[61] Lampinen M.J. - Noponen T., *Thermodynamic analysis of the interaction of the xylem water and phloem sugar solution and its significance for the cohesion theory.* Journal of Theoretical Biology, 224 (2003) 285–298

[62] Lide D. R., *Handbook of Chemistry and Physics, 85th Edition.* CRC Press, Boca Raton (2004).

[63] Lutsko J.M., *Density functional theory of inhomogeneous liquids. I. The liquid-vapour interface in Lennard-Jones fluids*, J. Chem. Phys., 127 (2007) 054701.

[64] Mackay J.F.G. - Weatherley P.E., *The effects of transverse cuts through the stems of transpiring woody plants on water transport and stress in the leaves.* Journal of Experimental Botany, 24 (1973) 15–28.

[65] Mattia D. - Gogotsi Y., *Review: static and dynamic behavior of liquids inside carbon nanotubes.* Microfluid-Nanofluid, 5 (2008) 289–305.

[66] McCarthy D.F., *Essentials of Soil Mechanics and Foundation. Basic Geotechnics.* Prentice Hall, Upper Saddle River (1988).

[67] McCully M.E. - Huang C.X. - Ling L.E.C., *Daily embolism and refilling of xylem vessels in the roots of field-grown maize*. New Phytologist, 138 (1998) 327-342.

[68] Mercury L. - Shmulovich K.I., *Experimental superheating and cavitation of water and solutions at spinodal-like negative pressures*. in: Transport and Reactivity of Solutions in Confined Hydrosystems. L. Mercury, N. Tas, Z. Michael, Eds., Springer, New York (2013) 158–171.

[69] Meyra A.G. - Kuz V.A. - Zarragoicoechea G.J., *Geometrical and physicochemical considerations of the pit membrane in relation to air seeding: the pit membrane as a capillary valve*. Tree Physiology, 27 (2007) 1401-1405.

[70] Milburn J.A. - Johnson R.P.C., *The conduction of sap II. Detection of vibrations produced by sap cavitation in Ricinus xylem*. Planta, 69 (1966) 43–52.

[71] Münch E. *Die Stoffbewegungen in der Pflanze*. Jena, Ger., Fischer, (1930).

[72] Nakanishi H. - Fisher M.E., *Multicriticality of wetting, prewetting, and surface transitions*. Phys. Rev. Lett., 49 (1982) 1565–1568.

[73] Nardini A. - Lo Gullo M.A. - Salleo S., *Refilling embolized xylem conduits: Is it a matter of phloem unloading?* Plant Science, 180 (2011) 604–611.

[74] O'Brien T.P. - Carr D.J., *A suberized layer in the cell walls of the bundle sheath of grasses*. Australian Journal of Biological Science, 23 (1970) 275–287.

[75] Ono S. - Kondo S., *Molecular theory of surface tension in liquid*. In: Structure of Liquids, S. Flügge, ed., Encyclopedia of Physics, X, Springer, Berlin (1960).

[76] Oron A. - Davis S.H. - Bankoff S.G., *Long-scale evolution of thin liquid films*. Rev. Mod. Phys., 69 (1997) 931-980.

[77] Pismen L.M. - Pomeau Y., *Disjoining potential and spreading of thin liquid layers in the diffuse-interface model coupled to hydrodynamics*. Phys. Rev. E, 62 (2000) 2480-2492.

[78] Preston R.D., *Movement of water in higher plants*. In: A. Frey-Wyssling, ed., Deformation and Flow in Biological Systems, North Holland Publishing (1952) 257–321.

[79] Preston R.D., *Tall for its age - Climbing a record breaking redwood*. The New Yorker (2006).

[80] Pridgeon A.M., *Diagnostic anatomical characters in the Pleurothallidinae (Orchidaceae)*. American Journal of Botany, 69 (1982) 921–938.

[81] Rocard Y., *Thermodynamique*. Masson, Paris (1987).

[82] Rowlinson J.S. - Widom B., *Molecular Theory of Capillarity*. Clarendon Press, Oxford (1984).

[83] Ruggeri T., *Introduzione alla Termomeccanica dei Continui*, Monduzzi, Milano (2007).

[84] Scholander P.F. - Love W.E. - Kanwisher J.W., *The rise of sap in tall grapevines*. Plant Physiology, 30 (1955) 93–104.

[85] Sheludko A., *Thin liquid films*. Advance in Colloid Interface Science, 1 (1967) 391–464.

[86] Seppecher P., *Equilibrium of a Cahn and Hilliard fluid on a wall: influence of the wetting properties of the fluid upon stability of a thin liquid film*. Eur. J. Mech. B/fluids, 12 (1993) 61–84.

[87] Serrin J., *Mathematical principles of classical fluid dynamics*, Encyclopedia of Physics, VIII/1. Springer, New York (1959).

[88] Sperry J.S., *Cutting-edge research or cutting-edge artefact? An overdue control experiment complicates the xylem refilling story*. Plant Cell and Environment, 36 (2013) 1916–1918.

[89] Stone H.A. - Stroock A.D. - Ajdari A., *Engineering flows in small devices: microfluidics toward a lab-on-a-chip*. Annual Review of Fluid Mechanics, 36 (2004) 381-411.

[90] Stroock A.D. - Pagay V.V. - Zwieniecki M.A. - Holbrook N.M., *The physicochemical hydrodynamics of vascular plants*. Annual Review of Fluid Mechanics, 46 (2014) 615–642.

[91] Tabeling P., Ed., *Microfluidics*. Comptes Rendus Physique, 5 (2004) 2–608.

[92] Truskinovsky L., *Equilibrium phase boundaries*. Sov. Phys. Dokl., 27 (1982) 551-553.

[93] Turgeon R., *The puzzle of phloem pressure*. Plant Physiology, 154 (2010) 578-581.

[94] Tyree M.T. - Dixon M.A., *Cavitation events in Thuja occidentalis L: Ultrasonic acoustic emissions from the sapwood can be measured*. Plant Physiology, 72 (1983) 1094-1099.

[95] Tyree M.T. - Sperry J.S., *Vulnerability of xylem to cavitation and embolism*. Annual Review of Plant Physiology and Plant Molecular Biology, 40 (1989) 19–38.

[96] Tyree M.T., *The cohesion-tension theory of sap ascent: current contreversies*, J. Exp. Botany, 48 (1997) 1753–1765.

[97] Tyree M.T. - Zimmermann M.H., *Xylem structure and the ascent of sap*. Springer, New York (2002).

[98] Tyree M.T. - Cochard H. - Cruiziat P., *The water-filled versus air-filled status of vessels cut open in air: The 'Scholander assumption' revisited*. Plant, Cell & Environment, 26 (2003) 613–621.

[99] van der Honert T.H., *Water transport in plants as a catenary process*. Discussions of the Faraday Society, 3 (1948) 1105–1113.

[100] van der Waals J.D., *The thermodynamic theory of capillarity under the hypothesis of a continuous variation of density*. Translation by J. S. Rowlinson, J. Statist. Phys., 20 (1979) 197-244.

[101] Weiss V.C., *Theoretical description of the adsorption and the wetting behavior of alkanes on water*. J. Chem. Phys., 125 (2006) 084718.

[102] Wenzel T.N., *Surface roughness and contact angle*. J. Phys. Colloid. Chem., 53 (1949) 1466.

[103] Wheeler T.D. - Stroock A.D., *The transpiration of water at negative pressures in a synthetic tree*. Nature, 55 (2008) 208–212.

[104] Widom B., *What do we know that van der Waals did not know?* Physica A, 263 (1999) 500–515.

[105] Zeppel M. J. B. - Murray B. R. - Barton C. - Eamus D., *Seasonal responses of xylem sap velocity to VPD and solar radiation during drought in a stand of native trees in temperate Australia*. Functional Plant Biology, 31 (2004) 461470.

[106] Zimmermann M.H., *Xylem Structure and the Ascent of Sap*. Springer, New York (1983).

[107] Zimmermann U. - Haase A. - Langbein D. - Meinzer F., *Mechanism of long-distance water transport in plants: a re-examination of some paradigms in the light of new evidence*. Phil. Trans. Roy. Soc. London, 431 (1993) 19–31.

[108] Zufferey V. - Cochard H. - Ameglio T. - Spring J.L. - Viret O., *Diurnal cycles of embolism formation and repair in petioles of grapevine (Vitis vinifera cv. Chasselas)*. Journal of Experimental Botany, 62 (2011) 3885–3894.

[109] Zwieniecki M.A. - Holbrook N.M., *Diurnal variation in xylem hydraulic conductivity in white ash (Fraxinus americana L.) red maple (Acer rubrum L.) and red spruce (Picea rubens Sarg.)*. Plant Cell Environ., 21 (1998) 1173-1180.

[110] Zwieniecki M.A. - Holbrook N.M., *Bordered pit structure and vessel wall surface properties: implications for embolism repair*. Plant Physiology, 123 (2000) 1015-1020.

[111] Zwieniecki M.A. - Holbrook N.M., *Confronting Maxwell´ s demon: biophysics of xylem embolism repair*. Trends in Plant Science, 14 (2009) 530-534.